Characterization of plastic limit surface and bifurcation domain of geomaterials

Florent Prunier [a], Jérôme Duriez [b], Luc Sibille [c] & Félix Darve [c]

[a] *Université de Lyon, INSA de Lyon, laboratoire GEOMAS, France*
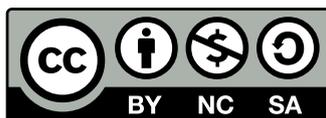
[b] *INRAE, Aix Marseille Univ, RECOVER, Aix-en-Provence, France*

[c] *Université Grenoble Alpes, laboratoire 3S-r, France.*

Abstract. Instabilities and failure in ductile non associated materials have been widely investigated during last decades especially in the case of geomaterials. It has been shown experimentally that collapse of some specimens can occur strictly within the ultimate plasticity limit, which is experimentally characterized by the maximum shear stress in a drained triaxial test. From a theoretical point of view such instability problems are well described using the so called second order work criterion derived from the Hill's stability analysis (Hill [1958]). Hence a question arises as to the experimental characterization of the ultimate plasticity limit with respect to the choice of stress paths. After a few reminders on Hill's theory, we prove in a general framework that the drained triaxial paths allow to determine with certainty this ultimate plasticity limit without any risk of preliminary bifurcation whatever the elasto-plastic material considered. We conclude that the plasticity limit is only slightly sensitive to variation of the internal state of the material, which can be described by different micromechanical quantities such as the void ratio and the fabric tensor. Furthermore, we define the limit of the bifurcation domain as the surface drawn in the 6-dimensional stress space that delimits the unconditionally stable space from the one where instabilities and failures can occur within the plasticity limit. However, we show that this latter limit is itself very sensitive to the evolution of the internal state of the soil sample.

Keywords. geomaterials, stability, plasticity limit characterization, bifurcation
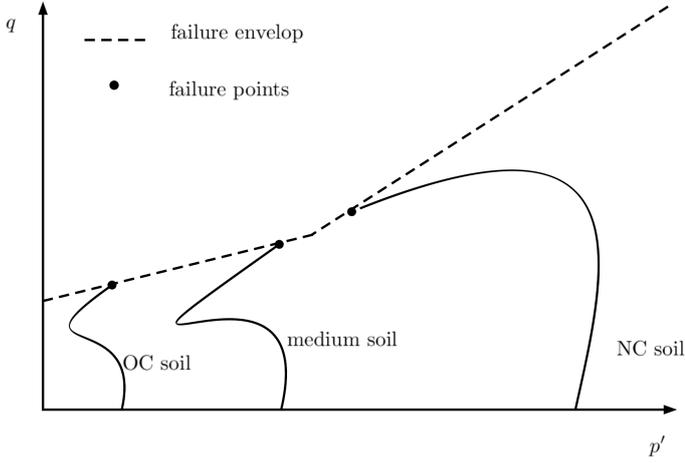
Figure 1. Sketch of the responses of a normally consolidated and an over consolidated soils samples according to an undrained triaxial compression.

1. Introduction

The behavior of geomaterials is complex, and it is now well known that loss of stability and failures can arise strictly within their plasticity limit (Darve and Vardoulakis [2004], Lade [1992], Nova [1991]). From a theoretical point of view, the plasticity limit is the surface plotted in the $6D$ stress space which bounds the admissible stress states of the material. For geomaterials, this limit is generally characterized with triaxial tests or direct shear tests. For soils with a low permeability, undrained triaxial tests are likely to be performed. On this particular stress path, normally consolidated materials exhibit a peak in the $(q - p')$ plane before reaching the plasticity limit obtained in drained conditions. In the rest of the paper we consider the axis 1 to be the major principal stress and the axis 3 to be the minor principal stress. We denote in a standard way $q = \sigma_1 - \sigma_3$ and $p = \mathrm{tr}(\boldsymbol{\sigma})/3$. It has been shown that from this peak the material is in an unstable state (Darve and Chau [1987], Darve and Vardoulakis [2004], Lade [1992], Nova [1991, 1994, 2004]). Indeed, we will see in section 3 that a collapse can be triggered if the test is stress driven. The Figure 1 shows a sketch of the responses of a soil sample according to an undrained triaxial test in an over consolidated state and in a normally consolidated state. Based on this simple fact the following question arise:

Q How to characterize properly the ultimate plasticity limit from an experimental point of view? In other words, how to define a proper loading path where the failure is reached on the plasticity limit without a previous loss of stability?

In order to answer this question, we will remain within a phenomenological framework in order to provide practical solutions that are relatively simple for an experimenter, even though great advances have been made in micromechanics over the last decade, either from a theoretical point of view using DEM simulation (Zhao et al. [2022], Farahnak et al. [2024], Wang et al. [2024]), or with new observations thanks to the development of tomographic imaging (Pinzon et al.

[2023], Cui et al. [2025]).

We first recall some general properties of rate independent materials and qualitatively describe the Octolinear model of Darve et al. [1995] in section 2 which is used in this work for illustrative purposes only. It should be emphasized that the approach described in this article is very general and not specific to any particular material. The only assumption is that the material is rate independant. For this approach to be useful, the material must also be non-associated, otherwise the material will remain unconditionally stable up to the plastic limit. Next, we recall the current knowledge on stability analysis of geomaterials using the second order work criterion in section 3. In section 4 we provide an answer to the main question posed above. Before closing the discussion of this paper, we provide in section 5 a description of the shape of the instability cones lying on the plasticity limit. In fact, unstable loading directions for stress states lying on the plasticity limit can be derived from an analytical manner and was never investigated before the present work. As recalled in the section 3, an instability cone is the set of loading directions that leads the material into an unstable state even inside the plasticity limit. Finally, we propose a discussion about the sensitivity of the limit of the bifurcation domain with the evolution of the internal state of the material. The bifurcation domain limit is the surface drawn in the $6D$ loading space that delimits the space where instability cones exist.

2. Short description of the elasto-plastic model used for the illustrations of the paper

This model is not based on the classical assumption of decomposition of the strain in an elastic plus a plastic part. It is instead, built from the general expression of rate independent models:

$$d\varepsilon_\alpha = N_{\alpha\beta}(u_\gamma)\,d\sigma_\beta \mid u_\gamma = \frac{d\sigma_\gamma}{\|d\boldsymbol{\sigma}\|} \qquad (1)$$

α, β, γ are indices $\in [1...6]$ when writing second order tensors $\boldsymbol{\sigma}$ and $\boldsymbol{\varepsilon}$ under a six columns vector form. The Einstein convention is used for repeated indices like β. From a general point of view, the 6 functions $N_{\alpha\beta}d\sigma_\beta$ respect the three mathematical properties to properly describe rate independent behaviors (Darve and Labanieh [1982], Darve et al. [1995]):

(1) they are homogeneous function of first order:

$$\forall \lambda \in \mathbb{R}^+ \; N_{\alpha\beta}(\lambda d\sigma_\beta) = \lambda N_{\alpha\beta}d\sigma_\beta \qquad (2)$$

This ensure that the response of the material is independent of the rate of the solicitation.

(2) they are non linear since $N_{\alpha\beta}$ depend on $u_\gamma = d\sigma_\gamma/\|d\boldsymbol{\sigma}\|$. This ensures the non reversibility of the response of the material

(3) they are anisotropic

Furthermore, the operator $\boldsymbol{N}$ depends on the previous loading history through memory parameters $\boldsymbol{h}$. A development in series limited to the second order of $\boldsymbol{N}$ gives the general

expression of incrementally non linear models of second order:

$$d\varepsilon_\alpha = N^1_{\alpha\beta} d\sigma_\beta + \frac{1}{\|d\boldsymbol{\sigma}\|} N^2_{\alpha\beta\gamma} d\sigma_\beta d\sigma_\gamma$$
$$\text{with } (\alpha, \beta, \gamma = 1, ..., 6) \tag{3}$$

Darve's constitutive model is obtained with three more assumptions :

- $\boldsymbol{N}$ is orhtotropic
- $d\sigma_\beta d\sigma_\gamma = 0$ for $\beta \neq \gamma$
- Shear moduli are incrementally linear (their expression not used in the present paper is described in Darve et al. [1995])

This leads to the incrementally non linear model of Darve expressed in identical principal axes:

$$\begin{Bmatrix} d\varepsilon_1 \\ d\varepsilon_2 \\ d\varepsilon_3 \end{Bmatrix} = \frac{1}{2} \left[N^+ + N^- \right] \begin{Bmatrix} d\sigma_1 \\ d\sigma_2 \\ d\sigma_3 \end{Bmatrix} + \frac{1}{2\|d\boldsymbol{\sigma}\|} \left[N^+ - N^- \right] \begin{Bmatrix} d\sigma_1^2 \\ d\sigma_2^2 \\ d\sigma_3^2 \end{Bmatrix} \tag{4}$$

with

$$N^\pm = \begin{bmatrix} \frac{1}{E_1^\pm} & -\frac{v_2^{1\pm}}{E_2^\pm} & -\frac{v_3^{1\pm}}{E_3^\pm} \\ -\frac{v_1^{2\pm}}{E_1^\pm} & \frac{1}{E_2^\pm} & -\frac{v_3^{2\pm}}{E_3^\pm} \\ -\frac{v_1^{3\pm}}{E_1^\pm} & -\frac{v_2^{3\pm}}{E_2^\pm} & \frac{1}{E_3^\pm} \end{bmatrix} \tag{5}$$

Fonctions E_i^+ and v_i^{j+} are defined on generalized triaxial loading paths when $d\sigma_i > 0$ and $d\sigma_j = d\sigma_k = 0$. Respectively E_i^- and v_i^{j-} are defined on generalized triaxial loading paths when $d\sigma_i < 0$ and $d\sigma_j = d\sigma_k = 0$. For $d\sigma_i = 0$, it can be verified that the relation is continuous (Gudehus [1979]). This latest model is not used in this document in order to keep analytical developments in relation with the illustrations. We can then remark that in one dimension, this relation is incrementally piecewise linear (one modulus for loading and another one for unloading):

$$d\varepsilon = \frac{1}{2} \left(\frac{1}{E^+} + \frac{1}{E^-} \right) d\sigma + \frac{1}{2} \left(\frac{1}{E^+} - \frac{1}{E^-} \right) |d\sigma| \tag{6}$$

By extrapolation, Darve defined the octolinear relation (eight tensorial zones) which is incrementally piecewise linear. A tensorial zone is a part of the incremental loading space where the constitutive model is linear. Using prior notations, the octolinear model is written as follows:

$$\begin{Bmatrix} d\varepsilon_1 \\ d\varepsilon_2 \\ d\varepsilon_3 \end{Bmatrix} = \frac{1}{2} \left[N^+ + N^- \right] \begin{Bmatrix} d\sigma_1 \\ d\sigma_2 \\ d\sigma_3 \end{Bmatrix} + \frac{1}{2} \left[N^+ - N^- \right] \begin{Bmatrix} |d\sigma_1| \\ |d\sigma_2| \\ |d\sigma_3| \end{Bmatrix} \tag{7}$$

In this expression, the eight tensorial zones are explicit, and the relationship 7 is identical to the following eight linear relations:

$$d\boldsymbol{\varepsilon} = (\boldsymbol{N_i})_{i=1,8} \, d\boldsymbol{\sigma} \tag{8}$$

with $(\boldsymbol{N_i})_{i=1,8}$ the matrix $\boldsymbol{N}$ where indices (+) are affected to the column (j) if $d\sigma_j > 0$, and (−) if $d\sigma_j < 0$ ($j \in \{1; 2; 3\}$).

For exemple, if $d\sigma_1 > 0$, $d\sigma_2 < 0$, $d\sigma_3 > 0$ we have:

$$N_2 = \begin{bmatrix} \frac{1}{E_1^+} & -\frac{v_2^{1-}}{E_2^-} & -\frac{v_3^{1+}}{E_3^+} \\ -\frac{v_1^{2+}}{E_1^+} & \frac{1}{E_2^-} & -\frac{v_3^{2+}}{E_3^+} \\ -\frac{v_1^{3+}}{E_1^+} & -\frac{v_2^{3-}}{E_2^-} & \frac{1}{E_3^+} \end{bmatrix} \tag{9}$$

In the next sections, this relation 8 will be used for analytical computations.

The empirical evolution of the various memory variables is not presented in this work, but the model tends asymptotically towards the Mohr-Coulomb failure criterion and describes a non associated flow rule. This model was mainly developed to describe the large deformation and cyclic behaviour of sands, but it has also been used to successfully reproduce the behaviour of clays (Darve and Labanieh [1982], Darve et al. [1986]). We also highlight that it was developed in a phenomelogical framework at the REV scale. The rules governing the evolution of the various constitutive variables depend on:

- the current void ratio
- the current stress state
- memory variables such as the values of the stress tensor components during a cycle change.

Hence, the evolution of the sample microstructure is not explicitly described by internal variables describing the fabric tensor or the tensor of the contact force distributions like it is done in some more recent models like Sanisand (Dafalias and Manzari [2004] or P2Psand Cheng and Detournay [2021]). This is done phenomenologically through the load history since a reference configuration, generally assumed to be isotropic. We point out that the evolution of the internal structure of a material is directly linked to its loading history from a reference state. These two notions are inseparable (Ouadfel and Rothenburg [2001]). It should also be noted that in the latest version of 1995 used in this work, the post-peak behaviour on a CD test and therefore the critical state for dense sands or over-consolidated clays is no longer described. Only asymptotic behaviour at the ultimate plasticity limit is described. In fact, it was considered in those years that the post-peak behaviour was not representative of the material because, in general, at least one discontinuity in the form of a shear band had developed. As a result, the sample is no longer homogeneous. Nevertheless, recent work analysing DEM results shows that within a shear band the microstructure stabilises in a remarkably stable configuration in the critical state (Zhu et al. [2016]). This attempts to prove the relevance of this concept. Moreover, it seems remarkable that it applies equally well to clays and granular materials. Nevertheless, this work does not focus on a detailed study of the behaviour of geomaterials, and despite the restrictions stated, the model used is sufficient to illustrate the main ideas and results of this work.

3. Background on the stability of non associated elasto-plastic materials

Failure in solid materials can be seen as a loss of the stability of the equilibrium state. The material is known as stable if a bounded load leads to a bounded response of the material, while at a failure state this response can be unbounded (Lyapunov [1907]). The most general criterion to describe such phenomena in elasto-plastic materials has been proposed by Hill [1958] and leads to the so called second order work criterion under small strains assumption and for homogeneous problems.

$$\forall (d\boldsymbol{\sigma}, d\boldsymbol{\varepsilon}) | d\boldsymbol{\sigma} = \mathcal{M}(d\boldsymbol{\varepsilon}), \quad w_2 = d\boldsymbol{\sigma} : d\boldsymbol{\varepsilon} > 0 \Rightarrow stability \tag{10}$$

with $\mathcal{M}(d\boldsymbol{\varepsilon})$ denoting the constitutive relationship linking $d\boldsymbol{\sigma}$ to $d\boldsymbol{\varepsilon}$. The condition 10 provides a sufficient condition of stability for the material. We will now analyse the condition.

$$w_2 = 0 \tag{11}$$

Using $\boldsymbol{N}$ the directional tangent operator (Gateaux [1913]) such that:

$$d\boldsymbol{\varepsilon} = \boldsymbol{N} d\boldsymbol{\sigma} \tag{12}$$

we get:

$$w_2 = 0 \Leftrightarrow d\boldsymbol{\sigma} : d\boldsymbol{\varepsilon} = d\boldsymbol{\sigma} \boldsymbol{N} d\boldsymbol{\sigma} = d\boldsymbol{\sigma} \boldsymbol{N_s} d\boldsymbol{\sigma} = 0 \tag{13}$$

$$\Leftrightarrow \frac{d\sigma_1^2}{E_1} + \frac{d\sigma_2^2}{E_2} + \frac{d\sigma_3^2}{E_3} - \left(\frac{v_1^2}{E_1} + \frac{v_2^1}{E_2}\right) d\sigma_1 d\sigma_2 - \left(\frac{v_1^3}{E_1} + \frac{v_3^1}{E_3}\right) d\sigma_1 d\sigma_3 - \left(\frac{v_3^2}{E_3} + \frac{v_2^3}{E_2}\right) d\sigma_3 d\sigma_2 = 0 \tag{14}$$

with $\boldsymbol{N_s}$ the symmetrical part of $\boldsymbol{N}$. Equation 14 is the general equation of an elliptical cone in the incremental principal stress space (Prunier et al. [2009c]). If we assume that at the virgin isotropic state all the eigenvalues of $\boldsymbol{N_s}$ are positive and they are then evolving continuously with the loading parameters, the following results hold:

- during the first loading steps all 3 eigenvalues are positive. Equation 14 has no solutions. The material is unconditionally stable.
- a first eigenvalues vanishes. Solution of Equation 14 is reduced to a single direction. If the loading path follows this particular direction the material is in an unstable state. The set of stress points such that the instability cone is reduced to a single direction define what we call the limit of the bifurcation domain (Darve et al. [2004], Darve and Vardoulakis [2004]). It is a surface plotted in the 6D stress space strictly included inside the plasticity limit for non associated materials ($\boldsymbol{N_s} \neq \boldsymbol{N}$). An illustration of such limit in the principal stress space is displayed on Figure 3.
- the lowest eigenvalue is negative and the two others are positive. Solution of Equation 14 is an elliptical cone. An illustration of such cones is presented on Figure 4. Due to the existence of tensorial zones for any rate independent material, these elliptical cones have to be truncated inside their own tensorial zone. If the loading path follows one of the particular directions include inside the cone (boundary included) the material is in an unstable state. The stress point is strictly inside the bifurcation domain.
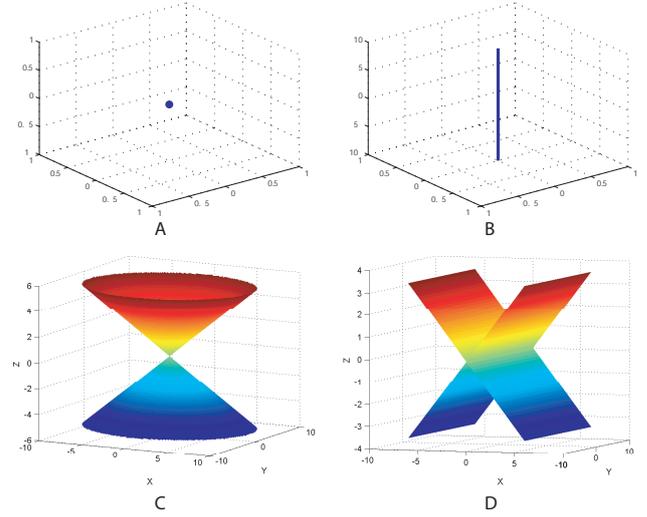
Figure 2. Shape of the solutions of equation 14 as a function of the sign of the eigenvalues. Eigenvalues are supposed to be initially all positive and are supposed to evolve continuously with the loading parameters. (A) $\lambda_1 > 0$, $\lambda_2 > 0$, $\lambda_3 > 0$. (B) $\lambda_1 > 0$, $\lambda_2 > 0$, $\lambda_3 = 0$. (C) $\lambda_1 > 0$, $\lambda_2 > 0$, $\lambda_3 < 0$. (D) $\lambda_1 > 0$, $\lambda_2 = 0$, $\lambda_3 < 0$
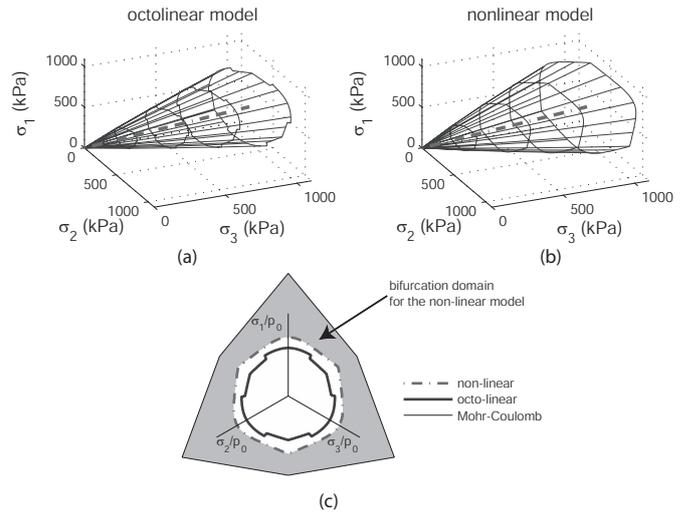
Figure 3. Bifurcation limit for the elasto-plastic models of Darve et al. [1995] calibrated on a dense sand.(Prunier et al. [2009a,b,c])

- the second eigenvalue vanishes (2 eigenvalues with opposite sign and one equal to zero). Solution of Equation 14 is the intersection of two planes. This last mathematical solution will be discussed later in the paper in relation with the cones that exist for stress points lying on the plasticity limit.

An illustration of such mathematical solutions is given in figure 2. Let us note that, the bifurcation domain and the instability cones can be also presented in the strain space (Prunier et al. [2009c]). Indeed, denoting

$$\boldsymbol{M} = \boldsymbol{N}^{-1} \tag{15}$$

Open Geomechanics, 2025, article no. 1

F. Prunier, J. Duriez, L. Sibille & F. Darve, *Characterization of plastic limit surface and bifurcation domain of geomaterials*   4
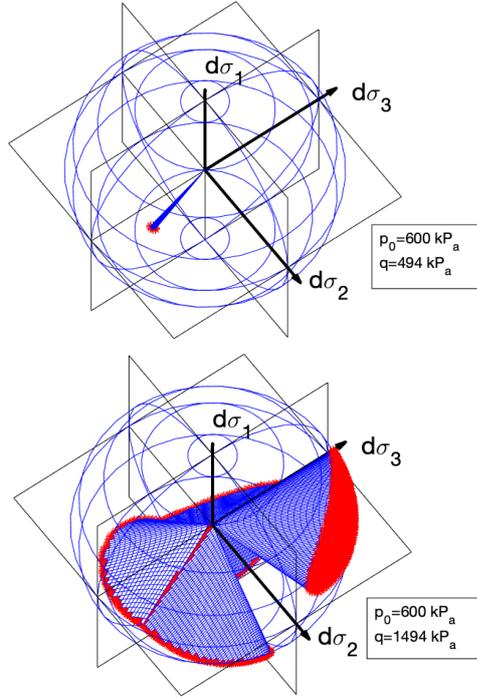
Figure 4. Some cones of unstable loading directions obtained with the Darve's model calibrated on a dense sand (Prunier et al. [2009a,b,c]). The first one is reduced to single direction and corresponds to a stress state on the bifurcation limit. The second one corresponds to a stress state within the bifurcation domain and strictly inside the plasticity limit.

and M_s its symmetric part, we get

$$w_2 = 0 \Leftrightarrow d\boldsymbol{\varepsilon} M d\boldsymbol{\varepsilon} = d\boldsymbol{\varepsilon} M_s d\boldsymbol{\varepsilon} = 0 \tag{16}$$

As a consequence it can be proved that the lowest eigen value of N_s vanishes at the same time than the one of M_s (Prunier et al. [2009a]).

It is worth noting that any loading direction corresponds to a particular loading path. In geotechnical applications, the most famous loading path which can lead to a failure inside the plasticity limit is the undrained triaxial path. This loading path is defined by the following relationships:

$$\begin{cases} d\varepsilon_1 = cst > 0 \\ d\varepsilon_1 + 2d\varepsilon_3 = 0 \end{cases} \tag{17}$$

Index $_1$ stands for axial direction and index $_3$ for radial direction. Along this loading path, the second order work can be rewritten with the conjugated variables of the test :

$$w_2 = d\boldsymbol{\sigma} : d\boldsymbol{\varepsilon} = dq \, d\varepsilon_1 + d\sigma_3 \, d\varepsilon_v \tag{18}$$

Due to the condition 17:

$$w_2 = dq \, d\varepsilon_1 \tag{19}$$

Thus, loose or normally consolidated soils are in unstable state when $dq \leqslant 0$ for this particular loading path. At the peak of q a generalized flow rule can be defined (Darve et al. [2004], Prunier et al. [2009a,b,c]). In fact, for such loading
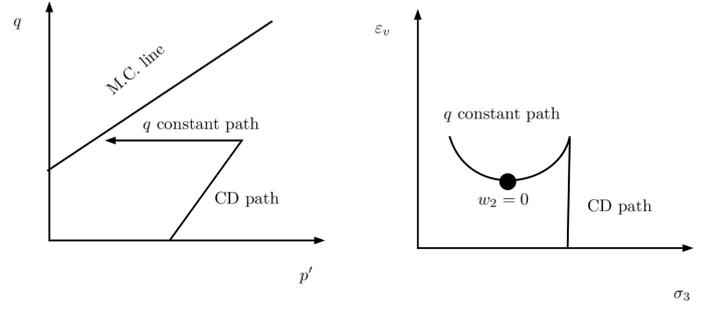
Figure 5. Sketch of the unloading path at constant q and typical response of some geomaterials to this path.

path, the incremental constitutive relationship can be written as follows :

$$S \begin{Bmatrix} d\varepsilon_1 \\ d\sigma_3 \end{Bmatrix} = \begin{Bmatrix} dq \\ d\varepsilon_v \end{Bmatrix} \tag{20}$$

with

$$S = \begin{bmatrix} E_1 & 2\frac{v_3^1}{E_3}E_1 - 1 \\ 1 - 2v_1^3 & \frac{2}{E_3}\left(1 - v_3 - 2v_3^1 v_1^3\right) \end{bmatrix} \tag{21}$$

The analytical expression of S is developed in appendix A. Hence when $dq = 0$, due to the relationship 17, we get :

$$S \begin{Bmatrix} d\varepsilon_1 \\ d\sigma_3 \end{Bmatrix} = \begin{Bmatrix} 0 \\ 0 \end{Bmatrix} \tag{22}$$

which defines what we call a generalized flow rule with the mixed variables $\begin{Bmatrix} d\varepsilon_1 \\ d\sigma_3 \end{Bmatrix}$ and the operator S.

$$\exists \begin{Bmatrix} d\varepsilon_1 \\ d\sigma_3 \end{Bmatrix} \neq \begin{Bmatrix} 0 \\ 0 \end{Bmatrix} \mid S \begin{Bmatrix} d\varepsilon_1 \\ d\sigma_3 \end{Bmatrix} = \begin{Bmatrix} 0 \\ 0 \end{Bmatrix} \tag{23}$$

As a consequence an effective failure occurs strictly inside the plasticity limit.

A second interesting particular loading path to be analysed is the q constant stress path. After a first loading path that provides a non zero deviatoric stress to the soil sample (like a drained triaxial path), a decrease of the mean stress is followed at constant deviator stress. An illustration of this stress path and a possible response of the material to this path is presented in Figure 5. Such stress path can be qualitatively typical of a rising water table, or of excavating works. In fact, for such applications some soil points are subjected to an unloading where the mean pressure decreases more quickly than the deviatoric one. To illustrate this purpose, we present some results of the simulation of a tunnel excavation in Appendix B.

This unloading at constant deviatoric stress can be defined with the following relationships:

$$\begin{cases} d\sigma_1' = cst < 0 \\ dq = 0 \end{cases} \tag{24}$$

because

$$dq = 0 \Leftrightarrow d\sigma_1' = d\sigma_3' = dp' \tag{25}$$

Along this stress path, the second order work can be rewritten with the conjugated variables of the test :

$$w_2 = d\boldsymbol{\sigma} : d\boldsymbol{\varepsilon} = d\sigma_1' \, d\varepsilon_v - 2d\varepsilon_3 \, dq \tag{26}$$

Due to the condition 24:

$$w_2 = d\sigma'_1 \, d\varepsilon_v \tag{27}$$

Along this stress path, the incremental constitutive relationship can be written as follows :

$$\boldsymbol{T}\begin{Bmatrix} d\sigma'_1 \\ -2d\varepsilon_3 \end{Bmatrix} = \begin{Bmatrix} d\varepsilon_v \\ dq \end{Bmatrix} \tag{28}$$

with

$$\boldsymbol{T} = \begin{bmatrix} \dfrac{1-4v_1^3}{E_1} + \dfrac{2v_1^3 v_3^1}{E_1(1-v_3)} & 2\dfrac{1-v_3-v_3^1}{1-v_3} \\ 1 + \dfrac{E_3}{E_1}\dfrac{v_1^3}{1-v_3} & -\dfrac{E_3}{2(1-v_3)} \end{bmatrix} \tag{29}$$

The expression of matrix $\boldsymbol{T}$ is developed in Appendix A. Hence when $d\varepsilon_v = 0$, due to the relationship 24, we get :

$$\boldsymbol{T}\begin{Bmatrix} d\sigma'_1 \\ -2d\varepsilon_3 \end{Bmatrix} = \begin{Bmatrix} 0 \\ 0 \end{Bmatrix} \tag{30}$$

A generalized flow rule is defined with the mixed variables $\begin{Bmatrix} d\sigma'_1 \\ -2d\varepsilon_3 \end{Bmatrix}$ and the operator $\boldsymbol{T}$

$$\exists \begin{Bmatrix} d\sigma'_1 \\ -2d\varepsilon_3 \end{Bmatrix} \neq \begin{Bmatrix} 0 \\ 0 \end{Bmatrix} \mid \boldsymbol{T}\begin{Bmatrix} d\sigma'_1 \\ -2d\varepsilon_3 \end{Bmatrix} = \begin{Bmatrix} 0 \\ 0 \end{Bmatrix} \tag{31}$$

Thus an effective failure occurs strictly inside the plasticity limit, but it is triggered with a strain component (extremum of ε_v) instead of a stress component.

In a more general framework, it is always possible to define a set of linear combinations of $d\boldsymbol{\sigma}$ and $d\boldsymbol{\varepsilon}$ as follows:

$$d\boldsymbol{\sigma}_{lc} = \boldsymbol{C}_\sigma d\boldsymbol{\sigma} \tag{32}$$

and

$$d\boldsymbol{\varepsilon}_{lc} = \boldsymbol{C}_\varepsilon d\boldsymbol{\varepsilon} \tag{33}$$

such that :

$$w_2 = d\boldsymbol{\sigma} : d\boldsymbol{\varepsilon} = d\boldsymbol{\sigma}_{lc} : d\boldsymbol{\varepsilon}_{lc} \tag{34}$$

The condition to get the effective failure inside the plasticity limit is that the test is driven with mixed parameters as follows :

$$\boldsymbol{F}\begin{bmatrix} d\boldsymbol{\varepsilon}^a_{lc} \\ d\boldsymbol{\sigma}^b_{lc} \end{bmatrix} = \begin{bmatrix} d\boldsymbol{\sigma}^a_{lc} \\ d\boldsymbol{\varepsilon}^b_{lc} \end{bmatrix} \tag{35}$$

with :

$$d\boldsymbol{\sigma}_{lc} = \begin{bmatrix} d\boldsymbol{\sigma}^a_{lc} \\ d\boldsymbol{\sigma}^b_{lc} \end{bmatrix} \tag{36}$$

and

$$d\boldsymbol{\varepsilon}_{lc} = \begin{bmatrix} d\boldsymbol{\varepsilon}^a_{lc} \\ d\boldsymbol{\varepsilon}^b_{lc} \end{bmatrix} \tag{37}$$

In fact, when :

$$\boldsymbol{F}\begin{bmatrix} d\boldsymbol{\varepsilon}^a_{lc} \\ d\boldsymbol{\sigma}^b_{lc} \end{bmatrix} = \begin{bmatrix} 0 \\ 0 \end{bmatrix} \tag{38}$$

along the loading path, $w_2 = 0$, a generalized flow rule is defined and an effective failure occurs. To conclude with this section, the conditions that enable failures strictly inside the plasticity limit are presented below.

(1) the stress point should be included inside the bifurcation domain
(2) the loading path should be inside (boundary included) the direction of one of the cones of unstable loading directions. These first two conditions are sufficient to get the loss of stability of the sample.

(3) the condition to get an effective failure is that conditions 1 and 2 are fulfilled and further more that the test is driven with proper mixed parameters.

4. A theoretical proper way to characterize the plasticity limit

In the framework of the elasto-plasticity theory recalled in section 3, the ultimate plasticity limit is defined with

$$det(\boldsymbol{M}) = 0 \tag{39}$$

with $\boldsymbol{M}$ the tangent operator such that :

$$d\boldsymbol{\sigma} = \boldsymbol{M} d\boldsymbol{\varepsilon} \tag{40}$$

while a failure that occurs inside this plasticity limit is defined with:

$$det(\boldsymbol{F}) = 0 \tag{41}$$

with $\boldsymbol{F}$ defined in a similar fashion than in equation 35. Furthermore some algebra allows to prove that (Prunier et al. [2009a,b,c]):

$$det(\boldsymbol{F}) \leqslant det(\boldsymbol{M}) \tag{42}$$

But from a practical point of view, constitutive relationships are characterized by analyzing some experimental tests. On these tests, the failure state has to be properly characterized, and we have to know if this failure state corresponds to an ultimate failure state lying on the plasticity limit or is a failure state that occurs inside the bifurcation domain.

In order to give practical answers to this problem, we propose to exploit the fact that for the associated materials the bifurcation domain limit and the plasticity limit coincide. Indeed in this last case we have $det(\boldsymbol{M}) = det(\boldsymbol{M_s}) = 0$ on the limit. To do so, we will answer to the following questions :

(1) Is it possible to define some loading path whose the part of the response of the material that provides the value of w_2 is independent of its associativity? In the exemple of the undrained triaxial loading path, only the response in term of dq gives the value of w_2, since $w_2 = dq d\varepsilon_1$ in this case (see equation 19). The response in term of $d\sigma_3$ does not affect w_2 since $d\varepsilon_v = 0$ by definition of the loading path. Nevertheless, w_2 depends on the associativity of the material along this loading path since w_2 never vanishes before the plasticity limit for dense sands and vanishes before for loose sands.
(2) When the existence of such loading paths is proved, can they scan every direction of the stress space to delineate experimentally the plasticity limit?

From a mathematical point of view a non associated material is characterized by the loss of its major symmetry on its tangent operator $\boldsymbol{M}$. Hence loading paths that answer question 1 are loading path whose the part of the response of the material which affect w_2 is independent of the symmetry of its tangent operator. From an obvious manner, a part of the set of these loading paths are any $1D$ loading path according the second order work. We can quote :

- simple compression / traction tests : $w_2 = d\sigma_1 d\varepsilon_1 + 2d\sigma_3 d\varepsilon_3 = d\sigma_1 d\varepsilon_1$ because $\sigma_3 = d\sigma_3 = 0$. What is essential in this particular case is that $w_2 = d\sigma_1^2/E_1$ which is independent of the associativity of the material. But these tests are useless for cohesionless geomaterials.
- drained triaxial tests : $w_2 = dq d\varepsilon_1 + d\sigma_3 d\varepsilon_v = d\sigma_1 d\varepsilon_1$, because $d\sigma_3 = 0$. And we also have $w_2 = d\sigma_1^2/E_1$ which is independent of the associativity of the material.

As a consequence, the q peak on a drained triaxial test characterizes properly an ultimate failure lying on the plasticity limit. In fact along such loading path, the response of the material in the plane $(q - \varepsilon_1)$ is independent of the associativity of the material. In other word, if it was possible to build two materials purely subjected to a Mohr-Coulomb model with the first one be associated $(\varphi = \psi)$ and the second one be non associated $(\varphi \neq \psi)$, their response in the (q, ε_1) will be strictly identical.

Standards axisymmetric tests do not allow to delineate the totality of the plasticity limit, but true $3D$ triaxial tests (Lanier et al. [1989]) defined by :

$$\begin{cases} d\varepsilon_1 = cst > 0 \\ d\sigma_2 = 0 \\ d\sigma_3 = 0 \\ \sigma_2^0 \neq \sigma_3^0 \end{cases} \tag{43}$$

allow such a characterization. Starting from the virgin isotropic state, a first drained triaxial path can be followed along the direction 2 or 3 to get $\sigma_2^0 \neq \sigma_3^0$ and the drained triaxial path can be then completed along the direction 1. As this loading program is not straightforward, loading paths at constant Lode's angle are generally preferred to characterize the $3D$ failure surface.

We are now interested in knowing if other loading paths defined experimentally provide values of w_2 which are independent of the associativity of the material. To do so, we introduce an avatar material such that :

$$\frac{v_i^{ja}}{E_i} = \frac{v_j^{ia}}{E_j} \quad \forall (i, j) \in [1, 3] \tag{44}$$

and

$$\frac{v_i^{ja}}{E_i} \neq \frac{1}{2}\left(\frac{v_i^j}{E_i} + \frac{v_j^i}{E_j}\right) \tag{45}$$

We are looking for particular loading directions in the $3D$ space of incremental principal stress such that :

$$w_2 = w_2^a \tag{46}$$

with w_2^a the value of the second order work of the avatar associated material as defined above.

For the sake of clarity we adopt a stepwise approach and first develop this idea for axisymmetric conditions. Let us introduce the stress proportional loading path :

$$\begin{cases} d\sigma_1 = cst \neq 0 \\ d\sigma_2 = d\sigma_3 \\ d\sigma_3 + Rd\sigma_1 = 0 \mid R \in \mathbb{R} \end{cases} \tag{47}$$

Due to the relationship 47, the second order works is written :

$$w_2 = d\sigma_1 (d\varepsilon_1 - 2Rd\varepsilon_3) \tag{48}$$

Injecting the constitutive relationship 85 plus the fact that $d\sigma_3 = -Rd\sigma_1$ we get :

$$w_2 = \left(\frac{2(1 - v_3)}{E_3}R^2 + 2\left(\frac{v_1^3}{E_1} + \frac{v_3^1}{E_3}\right)R + \frac{1}{E_1}\right)d\sigma_1^2 \tag{49}$$

In the same manner we find for the avatar associated material :

$$w_2^a = \left(\frac{2(1 - v_3)}{E_3}R^2 + \frac{4v_1^{3a}}{E_1}R + \frac{1}{E_1}\right)d\sigma_1^2 \tag{50}$$

Making $w_2 - w_2^a = 0$, we look for R such that:

$$R\left(\frac{v_1^3}{E_3} + \frac{v_3^1}{E_1}\right) = 2R\frac{v_3^{1a}}{E_1} \tag{51}$$

We can then easily conclude that under axisymmetric conditions only the value of $R = 0$ (that is too say the drained triaxial path) provides a loading path whose evolution of the second order work quantity is independent of the associativity of the material. Nevertheless this last condition is very strong. This means that without any knowledge of the material, it can be stated that no bifurcation can occur before reaching the plasticity limit during the test if the sample remains homogeneous. In fact, strain localisation can be observed for some materials just before reaching the maximum deviatoric stress for drained triaxial path. In the latter case, the material is no longer homogeneous and the stress-strain response at the boundary is not characteristic of the material behaviour. Furthermore, it can be proven that $w_2 = 0$ in a localized band when it appears (see Appendix C after Nicot and Darve [2011], Wan et al. [2017]). Questions of strain localization are not the purpose of this paper and will not be developed further in this work.

We will now investigate $3D$ conditions in the principal stress space:

$$\begin{cases} d\sigma_1 = cst \neq 0 \\ d\sigma_2 + R_1 d\sigma_1 = 0 \mid R_1 \in \mathbb{R} \\ d\sigma_3 + Rd\sigma_1 = 0 \mid R \in \mathbb{R} \end{cases} \tag{52}$$

For these stress paths, the expression of the second order work is:

$$w_2 = d\sigma_1 (d\varepsilon_1 - R_1 d\varepsilon_2 - Rd\varepsilon_3) + (d\sigma_2 + R_1 d\sigma_1) d\varepsilon_2 + (d\sigma_3 + Rd\sigma_1) d\varepsilon_3 \tag{53}$$

Injecting the constitutive relationship 84 plus the fact that $d\sigma_2 = -R_1 d\sigma_1$ and $d\sigma_3 = -Rd\sigma_1$ we get :

$$w_2 = \left(\frac{1}{E_1} + \frac{R_1^2}{E_2} + \frac{R^2}{E_3} - \left(\frac{v_3^2}{E_3} + \frac{v_2^3}{E_2}\right)R_1 R + \left(\frac{v_2^1}{E2} + \frac{v_1^2}{E_1}\right)R_1 + \left(\frac{v_3^1}{E_3} + \frac{v_1^3}{E_1}\right)R\right)d\sigma_1^2 \tag{54}$$

In the same manner we have for the avatar associated material :

$$w_2^a = \left(\frac{1}{E_1} + \frac{R_1^2}{E_2} + \frac{R^2}{E_3} - \frac{2v_3^{2a}}{E_3}R_1 R + \frac{2v_1^{2a}}{E_1}R_1 + \frac{2v_1^{3a}}{E_1}R\right)d\sigma_1^2 \tag{55}$$

Open Geomechanics, 2025, article no. 1

F. Prunier, J. Duriez, L. Sibille & F. Darve, *Characterization of plastic limit surface and bifurcation domain of geomaterials* 7

Making $w_2 - w_2^a = 0$, we look for R and R_1 such that:

$$\Phi(R, R_1) = \left(2\frac{v_3^{2a}}{E_3} - \frac{v_3^2}{E_3} - \frac{v_2^3}{E_2}\right)RR_1 - \tag{56}$$

$$\left(2\frac{v_1^{3a}}{E_1} - \frac{v_3^1}{E_3} - \frac{v_1^3}{E_1}\right)R - \left(2\frac{v_1^{2a}}{E_1} - \frac{v_2^1}{E_2} - \frac{v_1^2}{E_1}\right)R_1 = 0$$

The trivial solution is given for $R = R_1 = 0$ which corresponds to the $3D$ drained triaxial path. Else the reduction of the conic $\Phi(R, R_1)$ under its canonical form prove that general solutions are of hyperbolic shape. But these hyperbolic solutions depend on the directional tangent Young's moduli E_i and of directional tangent Poisson's ratio v_i^j which are not known a priori when performing an experimental test. Hence the detailed analysis of these hyperbolic solutions are useless in practice. Thus, we can conclude that only generalized $3D$ drained triaxial path allows a proper characterization of the plasticity limit for certainty. For the sake of clarity, the demonstration was based on the assumption of orthotropic behavior. But it's also simple to prove that w_2 cannot vanishes before reaching the plasticity limit for a generalized $6D$ drained triaxial direction in the case of general rate-independent behavior (see Appendix F).

Nevertheless, it is not always easy to perform a generalized drained triaxial path experimentally. In particular, radial stress paths in the deviatoric plane ar generally preferred to characterize the $3D$ plasticity limit (see eq. 52). In this last case, it is sufficient to plot the response of the material in term of $(\varepsilon_1 - R_1\varepsilon_2 - R\varepsilon_3)$ and to look if this variable is going through an extremum during the test (see expression of w_2 in equation 53). If not, w_2 remains strictly positive during the test and vanishes only on the plasticity limit because of the existence of the flow rule. Indeed, the flow rule states:

$$\exists d\boldsymbol{\varepsilon} \neq \mathbf{0}, \ \boldsymbol{M} \cdot d\boldsymbol{\varepsilon} = \mathbf{0} \tag{57}$$

as a consequence, $w_2 = 0$ for any loading direction toward the plasticity limit. We can then state that, the failure is reached on the plasticity limit without a previous bifurcation if the sample remain homogeneous. To illustrate this purpose we present the simulation of radial stress paths in the deviatioric plane to characterize experimentally the $3D$ Mohr-Coulomb envelop. These paths are at constant mean stress and constant Lode's angle θ. They can be defined with the following relationships :

$$\begin{cases} d\sigma_1 = cst\sqrt{\frac{2}{3}}\cos\theta \\ d\sigma_2 = -cst\left(\frac{1}{\sqrt{6}}\cos\theta + \frac{\sqrt{2}}{2}\sin\theta\right) \quad cst \in \mathbb{R}_+^* \\ d\sigma_3 = -cst\left(\frac{1}{\sqrt{6}}\cos\theta - \frac{\sqrt{2}}{2}\sin\theta\right) \end{cases} \tag{58}$$

with cst a strictly positive constant parameter. It is worth noting that these paths are particular ones of 52 with:

$$\begin{cases} R_1 = \frac{1}{2} + \frac{\sqrt{3}}{2}\tan\theta \\ R = \frac{1}{2} - \frac{\sqrt{3}}{2}\tan\theta \end{cases} \tag{59}$$

Since the Mohr-Coulomb failure criterion is isotropic (i.e. its expression is invariant to any change of reference frame), a series of simulations with $\theta \in [0, 60°]$ is sufficient to characterize the plasticity limit. On the figure 6 we present the
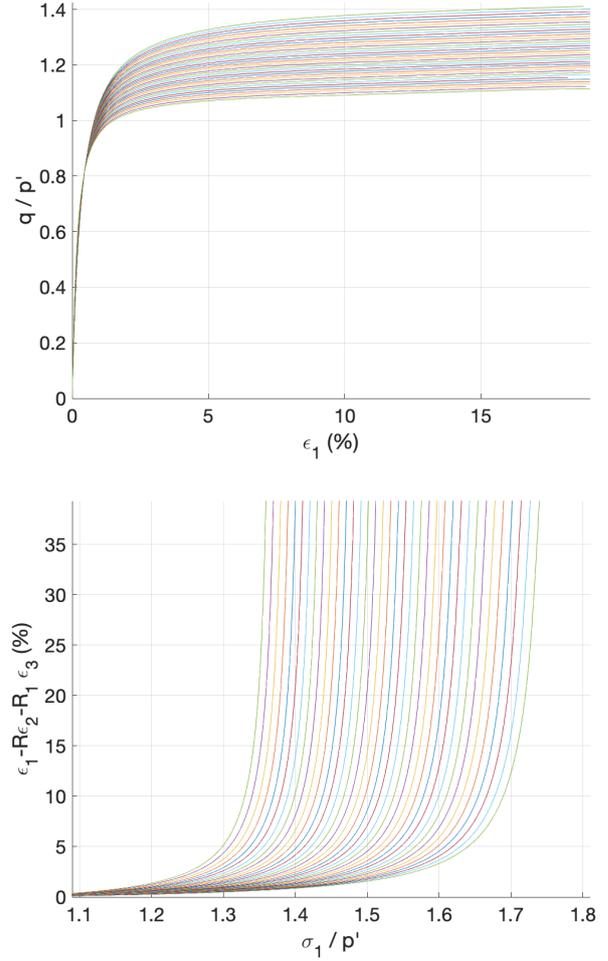
Figure 6. response of the octo-linear model calibrated on a dense Hostun sand to radial loading paths in the deviatoric plane. Response of the loose Hostun sand is displayed in Appendix D

response of 60 simulations using the octolinear model of Darve (Darve and Labanieh [1982], Darve et al. [1995]) calibrated on a dense Hostun sand, for illustrative purposes only without attempting to demonstrate general results. If these curves were derived from laboratory tests, we could conclude that the maximum value reached by σ_1 characterises the failure state at the ultimate plastic limit, because the response in terms of $(\varepsilon_1 - R_1\varepsilon_2 - R\varepsilon_3)$ does not show an extremum.

In conclusion, only drained triaxial tests can unequivocally characterize the plastic limit. Secondly, proportional stress tests can also be used if we ensure that no bifurcation has occurred beforehand by checking that $(\varepsilon_1 - R_1\varepsilon_2 - R\varepsilon_3)$ has not passed through an extremum. For proportional strain tests, such as the undrained test, this becomes complicated because :

(1) the maximum stress $(\sigma_1 - R_1\sigma_2 - R\sigma_3)$ can be reached before the plastic limit (q pic for the undrained axisymmetric test: $R_1 = R = 0.5$)

(2) the path generally tends to tangent the plasticity limit, which makes its characterization much less precise.

However, we agree that for materials with low permeability, the undrained triaxial test remains the simplest and most effective test to carry out to characterize the behavior of the material.

5. Discussion about the shape of instability cones lying on the plasticity limit

In former works, the shape of instability cones lying on the plasticity limit was not investigated. Moreover, the analytical solution of the equation 14 consisting of two intersecting planes has only been considered as an infinite elliptical cone and as a physically impossible limit state. That's why we follow the investigations in this work. In this section we also adopt a progressive approach by starting the investigation in axisymmetric conditions and then developing the idea in 3D conditions.

5.1. axi symmetric conditions

In axisymmetric conditions the tangent constitutive relationship reads:

$$\left\{ \begin{array}{c} d\varepsilon_1 \\ \sqrt{2}d\varepsilon_3 \end{array} \right\} = \left[\begin{array}{cc} \frac{1}{E_1} & -\sqrt{2}\frac{v_3^1}{E_3} \\ -\sqrt{2}\frac{v_1^3}{E_1} & \frac{1-v_3}{E_3} \end{array} \right] \left\{ \begin{array}{c} d\sigma_1 \\ \sqrt{2}d\sigma_3 \end{array} \right\} \quad (60)$$

Hence the equation of the instability cones gives:

$$w_2 = \frac{d\sigma_1^2}{E_1} + 2\frac{(1-v_3)}{E_3}d\sigma_3^2 - 2\left(\frac{v_1^3}{E_1} + \frac{v_3^1}{E_3}\right)d\sigma_1 d\sigma_3 \leqslant 0 \quad (61)$$

$$\Leftrightarrow d\sigma_1^2 + 2\frac{(1-v_3)E_1}{E_3}d\sigma_3^2 - 2\left(v_1^3 + \frac{v_3^1 E_1}{E_3}\right)d\sigma_1 d\sigma_3 \leqslant 0 \quad (62)$$

On the plasticity limit one Young's modulus vanishes since:

$$\det(M) = \frac{E_1 E_3}{1 - v_3 - 2v_1^3 v_3^1} \quad (63)$$

Let us assume that:

$$E_1 = 0 \quad (64)$$

we get :

$$d\sigma_1^2 - 2v_1^3 d\sigma_1 d\sigma_3 \leqslant 0 \quad (65)$$

$$\Leftrightarrow d\sigma_1 \left(d\sigma_1 - 2v_1^3 d\sigma_3 \right) \leqslant 0 \quad (66)$$

This domain is then bounded by the two lines:

$$d\sigma_1 = 0 \quad (67)$$

and

$$d\sigma_1 - 2v_1^3 d\sigma_3 = 0 \quad (68)$$

Let us now detail this domain:

$$d\sigma_1 - 2v_1^3 d\sigma_3 \leqslant 0 \quad (69)$$

$$\Leftrightarrow \frac{d\sigma_1}{d\sigma_3} \leqslant 2v_1^3 \quad \text{if } d\sigma_3 > 0 \quad (70)$$

$$\Leftrightarrow \frac{d\sigma_1}{d\sigma_3} \geqslant 2v_1^3 \quad \text{if } d\sigma_3 < 0 \quad (71)$$

- $(\sigma_1; \sigma_3)$ lying on the plasticity limit
- unstable directions
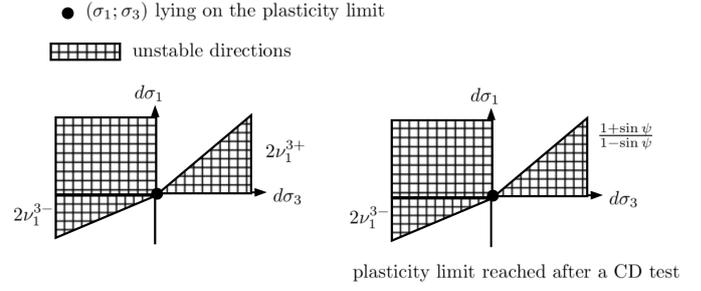
Figure 7. instability secant planes (degenerated cones with an infinite wider axis) for a stress state lying on the plasticity limit. Sum up of equations 66 to 77. 0, $2v_1^{3\pm}$ and $\frac{1+\sin\psi}{1-\sin\psi}$ are the slope of the instability secants planes.

When the plasticity limit is reached after a drained triaxial path, we have:

$$v_1^3 = -\left(\frac{d\varepsilon_3}{d\varepsilon_1}\right)_{d\sigma_3=0} = -\frac{d\varepsilon_3}{d\varepsilon_1} \quad (72)$$

For models based on the Mohr-Coulomb limit the ratio $d\varepsilon_3/d\varepsilon_1$ at failure allows to define the dilatancy angle ψ. The flow surface is simply defined by:

$$g : \sigma_1 - \frac{1+\sin\psi}{1-\sin\psi}\sigma_3 = 0 \mid \sigma_1 > \sigma_2 > \sigma_3 \quad (73)$$

and its normal

$$\vec{n} = \left\{ \begin{array}{c} 1 \\ 0 \\ -\frac{1+\sin\psi}{1-\sin\psi} \end{array} \right\} \mid \sigma_1 > \sigma_2 > \sigma_3 \quad (74)$$

allows to define the ratio $d\varepsilon_3/d\varepsilon_1$ at failure as a function of $\sin\psi$ for $\sigma_1 > \sigma_2 > \sigma_3$. For axisymmetric conditions, $\sigma_2 = \sigma_3$ and we assume:

$$\vec{n} = \frac{1}{2}\left\{ \begin{array}{c} 1 \\ 0 \\ -\frac{1+\sin\psi}{1-\sin\psi} \end{array} \right\} + \frac{1}{2}\left\{ \begin{array}{c} 1 \\ -\frac{1+\sin\psi}{1-\sin\psi} \\ 0 \end{array} \right\} \quad (75)$$

which is the bisector line of the normals of the two secant planes for the Lode's angle $\theta = 0$. This provides the following relationship for the flow direction:

$$\left(\frac{d\varepsilon_3}{d\varepsilon_1}\right)_{failure} = -\frac{1}{2}\frac{1+\sin\psi}{1-\sin\psi} \quad (76)$$

Combining equations 70, 72 and 76, we get the upper limit of the cone for a drained triaxial path :

$$\frac{d\sigma_1}{d\sigma_3} \leqslant \frac{1+\sin\psi}{1-\sin\psi} \quad \text{for } (d\sigma_1, d\sigma_3) \in \mathbb{R}_+^2 \quad (77)$$

We sum up the results between equation 66 and equation 77 on the figure 7. Nevertheless, the direction given by $2v_1^3$ does not necessarily matches the direction given by the plasticity limit itself. In fact for all directions crossing the plasticity limit we have $w_2 = 0$ since $Md\varepsilon = 0$. Hence the tangent to the plasticity limit surface is a cone of unstable loading directions open at 180°. As we assume here that the stress
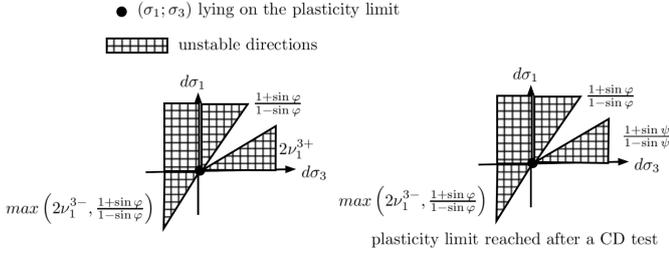
Figure 8. instability secant planes (degenerated cones with an infinite wider axis) for a stress state lying on the plasticity limit. Sum up of equations 66 to 77 and merging the plasticity limit condition. 0, $2\nu_1^{3\pm}$ and $\frac{1+\sin\psi}{1-\sin\psi}$ are the slope of the instability secants planes. $\frac{1+\sin\varphi}{1-\sin\varphi}$ is the slope of the Mohr-Coulomb plane.

point is lying on the plasticity limit, only neutral loading directions are authorized ultimately. For a Mohr-Coulomb criterion this neutral direction is given by:

$$\frac{d\sigma_1}{d\sigma_3} = \frac{1+\sin\varphi}{1-\sin\varphi} \qquad (78)$$

As a consequence we also have to merge the solutions of the instability cones shown in figure 7 with the tangent plane of the plasticity limit. Such final solution is given in figure 8.

5.2. 3D conditions

Starting from equation 14 which is the general equation of an elliptic cone, we know that this shape can degenerate to the one of the intersection of two planes when the maximum and the minimum eigenvalues are of opposite sign and when the intermediate one is zero. This is what happens for a stress state lying on the plasticity limit due to the fact that one Young's modulus vanishes. In fact we have:

$$\det(M) = \frac{E_1 E_2 E_3}{1 - \nu_1^2\nu_2^1 - \nu_1^3\nu_3^1 - \nu_2^3\nu_3^2 - \nu_1^2\nu_2^3\nu_3^1 - \nu_1^3\nu_3^2\nu_2^1} \qquad (79)$$

Let us assume that $E_1 = 0$ and introduce this condition directly inside the equation 14 by multiplying each term by E_1 we directly get the equations of these two secant planes:

$$d\sigma_1^2 - \nu_1^2 d\sigma_1 d\sigma_2 - \nu_1^3 d\sigma_1 d\sigma_3 = 0 \qquad (80)$$

$$\Leftrightarrow d\sigma_1\left(d\sigma_1 - \nu_1^2 d\sigma_2 - \nu_1^3 d\sigma_3\right) = 0 \qquad (81)$$

the first plane is then the horizontal plane given by the cartesian equation :

$$d\sigma_1 = 0 \qquad (82)$$

and the second one is the one given by the cartesian equation :

$$d\sigma_1 - \nu_1^2 d\sigma_2 - \nu_1^3 d\sigma_3 = 0 \qquad (83)$$

We have to notice that this two secant planes corresponds to the limit case of the elliptic cone with an infinite wider axis of the ellipse. As for the axisymmetric case this last plane does not necessarily matches the tangent plane of the plasticity limit, and the set of unstable loading directions have to be merged with the ones normal to the tangent plane of the plasticity limit. On figure 9 we present cones of unstable loading directions in the vicinity of the plasticity limit obtained with the octolinear model of Darve. In fact the
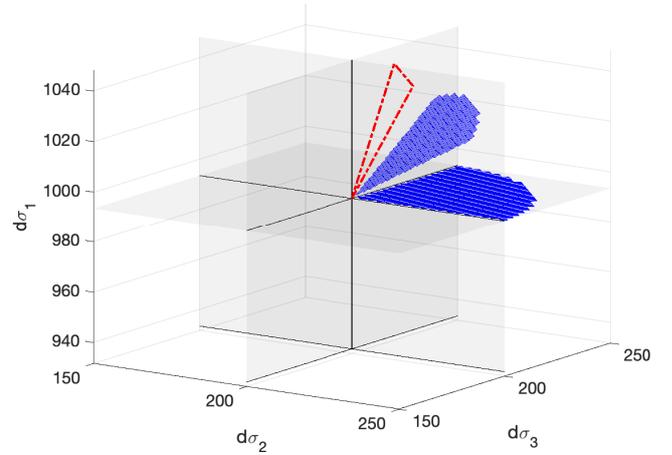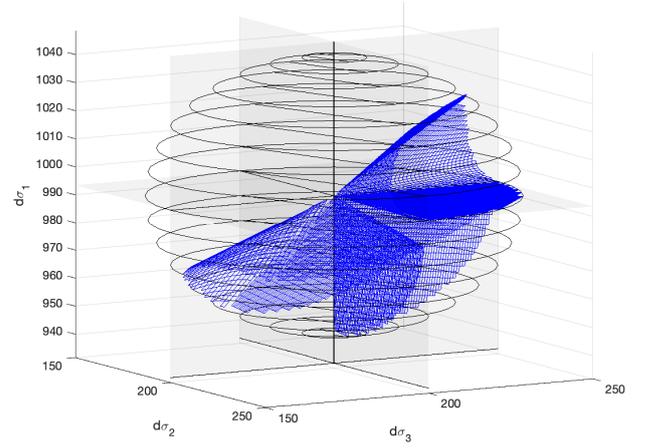
Figure 9. 3D instability cone get with the octolinear model of Darve for a stress point in the vicinity of the Mohr-Coulomb envelop. On th right figure we only kept the cone for the tensorial zone [$d\sigma_1$>0, $d\sigma_2$>0, $d\sigma_3$>0] and added the tangent plane to the Mohr-Coulomb envelop in dashed line.

plasticity limit is reached asymptotically with this model. Thus cones in each tensorial zone has been plotted using equation 14. On the right figure 9, we have kept only the cone in the tensorial zone ($d\sigma_1 > 0, d\sigma_2 > 0, d\sigma_3 > 0$). We can see that the elliptical cone is almost an intersection of two planes as shown from a mathematical point of view. We also added in dashed line the tangent plane corresponding to the plasticity limit. As in axisymmetric condition we can see that it is not coincident with the upper plane given by the equation 14.

In conclusion of this discussion, we can quote that the tangent plane to the plasticity limit can be viewed as an instability "cone" that opens suddenly at 180° in both tangential directions. In this sense it is distinct from the other instability cones that open continuously inside the bifurcation domain until to be opened in the form of two secant planes when reaching the plasticity limit. In our knowledge, instability cones have been studied with Darve's model, Pastor-Zienkiewicz's model (Pastor et al. [1990]), Plasol's

model (Barnichon [1998]), and a basic DEM model using spherical particles (Sibille et al. [2007]). The first two ones predict this upper right instability cone, while the two other ones don't. Because of the DEM model we were prone to think that this cone was an artifact of the Darve and Pastor-Zienkiewicz models, but this last analytical solution given for stress states lying on the plasticity limit encourage us to think that this upper right cone develops really continuously inside the bifurcation domain, before developing ultimately into two secant planes at the plasticity limit.

6. Discussion about the sensitivity of the limit of the bifurcation domain with the evolution of the internal state of the material

Experimental evidence shows that for geomaterials, the critical state characterised by a constant void ratio and a constant deviatoric stress for infinite deviatoric strain is a state independent of the initial internal state of the material. The plasticity limit at the critical state can therefore be described as unique. As for the ultimate plasticity limit (at the peak of the stress deviator), the experimental evidence clearly shows its dependence on the initial void ratio. Results presented with the discrete element method also prove that this limit depends on other more complex internal parameters (Zorzi et al. [2017]). However, this dependence seems limited when considering a given initial state and monotonic paths or even cyclic paths with a limited number of cycles. Indeed, from a initial reference configuration of the soil sample, a particular point on the plasticity limit is characteristic of a failure state after any loading paths that avoid every direction inside an instability cone. Now, we are interested in knowing if the limit of the bifurcation domain presented in figure 3 and characterized with a classical drained triaxial path can be also considered as a weakly depend surface with the internal state of the material. From an analytical point of view it is not obvious when looking at the equation 14. In fact eigenvalues of N_s depends on the evolutions of E_i and v_i^j $\left((i,j) \in [1,3]^2\right)$. Thus, the first unstable loading direction that appears may be strongly subject not only to the initial state of the material but also of the previous loading path. To investigate this point we have simulated a drained triaxial loading path stopped before reaching the plasticity limit in compression ($\varepsilon_1 \approx 2\%$) and we then imposed an unloading until the plasticity limit in extension. In figure 10, we have reported the response of the materials which is representative of a dense sand. The red crosses delimit the bifurcation domain in the compression phase while the yellow circles delimit the bifurcation domain in the unloading phase. Starting from the initial isotropic state, a first unstable direction appears at point A (see figure 12. Then instability cones grows and develop until point B. At this point we start the unloading. Instability cones shrink and reduce to a single direction in point C. Between points C and D we are in a fully stable domain: no instability cones exist. Finally a first unstable direction appears in point D which is in the vicinity of the hydrostatic
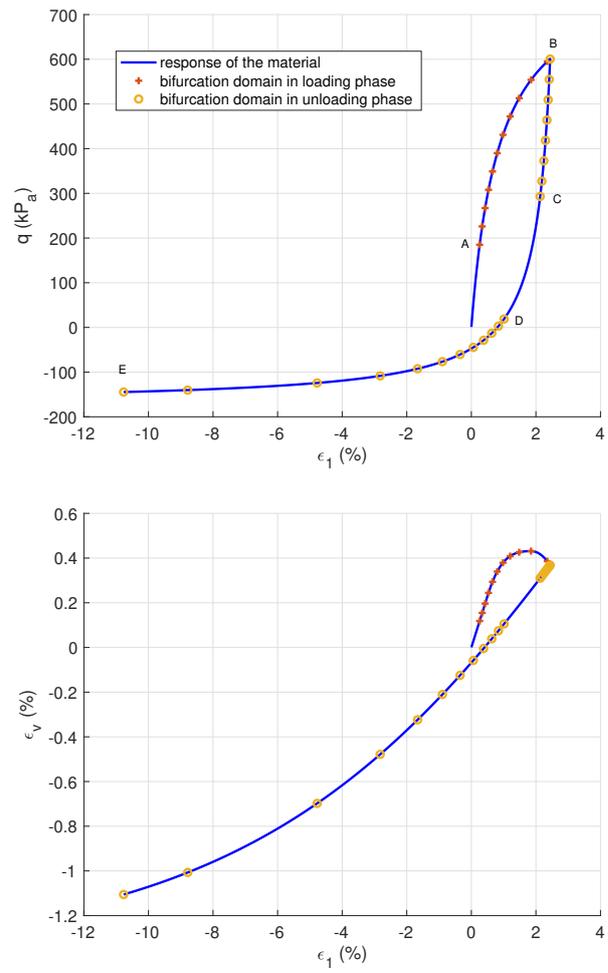
Figure 10. Response of the Octolinear model calibrated on a dense Hostun sand to an alternated drained triaxial path

stress lane. If this stress state was reached from a virgin initial hydrostatic state it would have been in a fully stable domain. This proves that the limit of the bifurcation domain is moving and deform with the evolution of the internal state of the material (which is characterized by the evolution of internal variables of elasto-plastic models). From point D instability cones are growing and developing until point E. Both bifurcation domains obtained from the initial isotropic state and the one obtained after the unloading are presented as function of the ratio q/p on the figure 11. As can be seen on this last figure, the limit of the bifurcation domain evolves strongly with the loading path and thus with the internal state of the material. The instability cones obtained at the points A, B, C, D, E are reported in figure 12. In appendix E, we present a similar simulation carried out with the same model calibrated on soft sand. The conclusions on the evolution of the bifurcation domain remain similar. Nevertheless, the response of such a material in the plane ($\varepsilon_v - \varepsilon_1$) is very different since a strong induced anisotropy develops as soon as the range $0\% \leqslant \varepsilon_1 \leqslant 2\%$ (see figure 18).
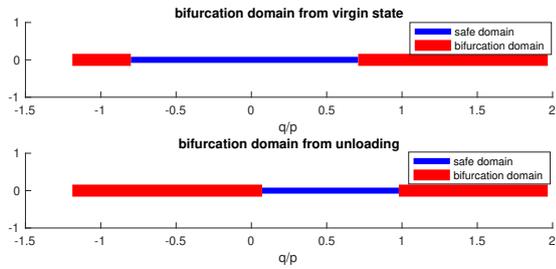
Figure 11. Evolution of the bifurcation domain for a dense sand. At the top, the bifurcation domain obtained starting from the initial isotropic state. At the bottom, the one obtained during the unloading.

These initial simulation results modestly show that for a model developed to describe the cyclic behaviour of granular materials such as sand, the limit of the bifurcation domain evolves continuously with the loading path. The experimental results on loose sands of Doanh et al. provide a first observations that could confirm this conclusion obtained with Darve's model. In their work, they carry out a series of undrained tests (CU+u) on very loose sands. The first was standard, but for the others they first prestress the sample with a drained test (CD) at a defined shear ratio $\eta = q/p'$. The higher the shear ratio η, the more similar the qualitative undrained response is to a dense sand. The authors emphasise that after the prestressing phase, the void ratio didn't change much and always remained around 0.9. (see figure 13). They prove that a loose sand can be stable until reaching the plasticity limit along a C.U+u path. These results go in the direction of a strong evolution of the bifurcation domain limit with the evolution of the internal state of the sample, even if no directional research can be carried out experimentally.

The results presented in figure 10 show that an hydrostatic stress state is found in the bifurcation domain after a single unloading cycle with the octo-linear model. This should be validated experimentally, but this would be very complicated to do because of the directional research required. Failing that, future work will be carried out with different discrete element models in order to validate these two observations:

(1) the evolution of the bifurcation domain limit with the loading path
(2) some particular granular assembly could be potentially unstable under an hydrostatic (or nearly hydrostatic) stress state

Despite the lack of validation of these results, we can make some remarks on writing constitutives models for soils. The simplest models are based on a yield surface with an isotropic strain hardening. For these models, when starting from an isotropic virgin state, the initial bifurcation domain limit can be close to the initial yield limit without being confused with it. Then once the initial bifurcation domain limit is passed, this boundary is always confused with the current yield limit. In fact, the bifurcation domain becomes smaller as the strain hardening proceeds and ultimately merges
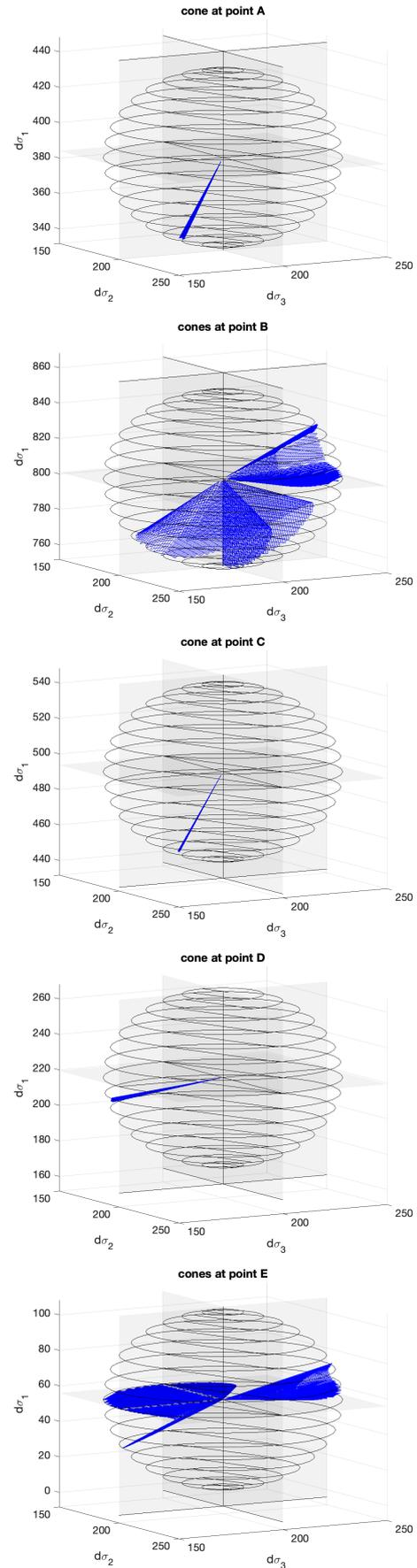
Figure 12. Development of instability cones along the stress path for the dense sand.
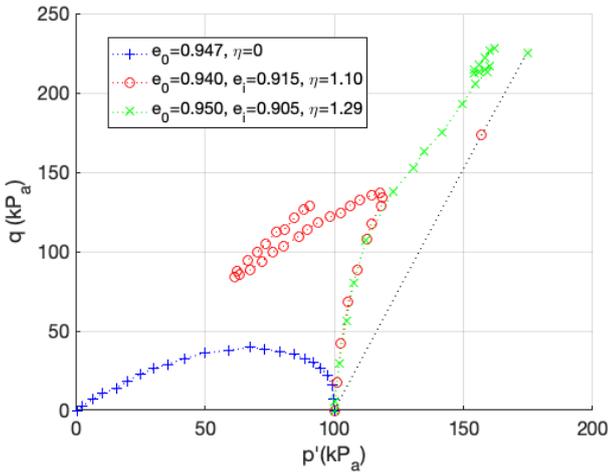
Figure 13. Experimental results on the Toyoura sand according to Doanh et al. [2013]. The first test '+' is a standard C.U+u test. The other two 'o' and 'x' are first prestressed C.D. tests until η 1.10 and η 1.29 respectively. They are then unstressed until η 0 and finally sheared to failure using the standard undrained procedure. e_0 denotes the void ratio at the end of the first isotropic consolidation pressure 100 kP_a, while e_i denotes the void ratio at p' 100 kP_a, but the end of the pre-shearing process.

with the plastic limit even if an unloading is subsequently performed. Consequently, it would be better to avoid using such models for any problem where some points may be unloaded with respect to the yield surface considered.

As a consequence, elasto-plastic models based on a kinematic strain hardening or hypo plasticity concept are better. But we understand that future work will have to be able to determine whether a non-infinitesimal radius of the elastic domain can be relevant from a physical point of view. Indeed, for a state located in the bifurcation domain, any unloading in the elastic radius is unconditionally stable. This loss of continuity of the evolution of the bifurcation domain limit with the loading parameters seems questionable.

7. Conclusion

In this paper we investigate the stability and failure of non-associated elasto-plastic materials such as geomaterials. We have recalled that in such materials effective instabilities and failures can develop strictly within the plasticity limit defined as the ultimate Mohr-Coulomb plasticity surface. Based on this observation, the question of the experimental characterisation of such an ultimate limit is addressed. We have proven in section 4 that true triaxial tests (with $\sigma_2^0 \neq \sigma_3^0$) allow the full characterisation of the plasticity limit like the Mohr-Coulomb surface with certainty. For non triaxial loading paths at constant mean stress and constant Lode's angle, it must be verified that no bifurcation occurred during the test as presented in section 4 in figure 6. Therefore we can say that the plasticity limit is only slightly

sensitive to variation of the internal state of the material. Indeed, starting from a given initial state this ultimate limit (mainly dependent of the initial configuration of the geomaterials) does not depend on the subsequent loading path. From a mathematical point of view it is characterised by the cancellation of one tangent Young's modulus of the tangent constitutive matrix. And the evolution of the tangent moduli along a loading path does not affect the non-associated character of the material. However, we have shown in section 6 that the Darve's octo-linear model can describe a strong evolution of the bifurcation domain limit with the loading path. In particular we have seen that this model predict that some material are inside the bifurcation domain under an isotropic stress state after a small loading-unloading drained triaxial path. It is worth noting that the existence of this bifurcation domain is conditioned by the induced anisotropy which develops in a non associated way ($v_i^j/E_i \neq v_j^i/E_j$) as it is the case for geomaterials. In this sense, this boundary is very sensitive to the evolution of the microstructure of the material with the loading.

We have recalled in section 5 that the instability cones develop continuously in the bifurcation domain. From this we have shown that their elliptical structure in the bifurcation domain degenerates into the intersection of two intersecting planes when the plasticity limit is reached. We have seen that one of this plane is the horizontal plane in the space $(d\sigma_1, d\sigma_2, d\sigma_3)$ when σ_1 is the highest principal stress. The second plane is between the tangent plane of the plasticity limit whose the direction is expressed in term of the friction angle φ and the horizontal plane. When the plasticity limit is reached after a triaxial path at $(d\sigma_2 = d\sigma_3 = 0)$ the direction of the second instability plane is defined with the dilatancy angle ψ. The tangent plane to the plasticity limit is a particular instability cone that arise suddenly with an opening at 180°, while the other ones develop continuously from a single direction, to an elliptical shape and ultimately to two secant planes that are distinct from the tangent plane to the plasticity limit. Hence it can be seen in future works if it exists a kind of a micro-mechanical signature of failures reached in a direction crossing the plasticity limit compared with the ones that hold for direction included in the other instability cones.

Appendix A.

For homogeneous laboratory tests where principal stress and principal strain axes coincide, the directional tangent constitutive relationship writes:

$$\begin{Bmatrix} d\varepsilon_1 \\ d\varepsilon_2 \\ d\varepsilon_3 \end{Bmatrix} = \begin{bmatrix} \frac{1}{E_1} & -\frac{v_2^1}{E_2} & -\frac{v_3^1}{E_3} \\ -\frac{v_1^2}{E_1} & \frac{1}{E_2} & -\frac{v_3^2}{E_3} \\ -\frac{v_1^3}{E_1} & -\frac{v_2^3}{E_2} & \frac{1}{E_3} \end{bmatrix} \begin{Bmatrix} d\sigma_1 \\ d\sigma_2 \\ d\sigma_3 \end{Bmatrix} \quad (84)$$

As a consequence, for axisymmetric conditions with $2 \equiv 3$ we get:

$$\begin{Bmatrix} d\varepsilon_1 \\ \sqrt{2} d\varepsilon_3 \end{Bmatrix} = \begin{bmatrix} \frac{1}{E_1} & -\sqrt{2}\frac{v_3^1}{E_3} \\ -\sqrt{2}\frac{v_1^3}{E_1} & \frac{1-v_3}{E_3} \end{bmatrix} \begin{Bmatrix} d\sigma_1 \\ \sqrt{2} d\sigma_3 \end{Bmatrix} \quad (85)$$

We are looking for the expression of the matrix S such that:

$$S \begin{Bmatrix} d\varepsilon_1 \\ d\sigma_3 \end{Bmatrix} = \begin{Bmatrix} dq \\ d\varepsilon_v \end{Bmatrix} \tag{86}$$

using relation 85 we get:

$$d\varepsilon_1 = \frac{1}{E_1} d\sigma_1 - 2\frac{v_3^1}{E_3} d\sigma_3 \tag{87}$$

and

$$d\varepsilon_v = \frac{1-2v_1^3}{E_1} d\sigma_1 + 2\frac{1-v_3-v_3^1}{E_3} d\sigma_3 \tag{88}$$

Using expressions 87 and 88 we can built matrices $\boldsymbol{\alpha}$ and $\boldsymbol{\beta}$ such that:

$$\begin{Bmatrix} d\varepsilon_1 \\ d\sigma_3 \end{Bmatrix} = \boldsymbol{\alpha} \begin{Bmatrix} d\sigma_1 \\ d\sigma_3 \end{Bmatrix} = \begin{bmatrix} \frac{1}{E_1} & -2\frac{v_3^1}{E_3} \\ 0 & 1 \end{bmatrix} \begin{Bmatrix} d\sigma_1 \\ d\sigma_3 \end{Bmatrix} \tag{89}$$

and

$$\begin{Bmatrix} dq \\ d\varepsilon_v \end{Bmatrix} = \boldsymbol{\beta} \begin{Bmatrix} d\sigma_1 \\ d\sigma_3 \end{Bmatrix} = \begin{bmatrix} 1 & -1 \\ \frac{1-2v_1^3}{E_1} & 2\frac{1-v_3-v_3^1}{E_3} \end{bmatrix} \begin{Bmatrix} d\sigma_1 \\ d\sigma_3 \end{Bmatrix} \tag{90}$$

Hence relationship 86 reads:

$$S\boldsymbol{\alpha} \begin{Bmatrix} d\sigma_1 \\ d\sigma_3 \end{Bmatrix} = \boldsymbol{\beta} \begin{Bmatrix} d\sigma_1 \\ d\sigma_3 \end{Bmatrix} \tag{91}$$

and

$$S = \boldsymbol{\beta}\boldsymbol{\alpha}^{-1} \tag{92}$$

with

$$\boldsymbol{\alpha}^{-1} = \begin{Bmatrix} E_1 & 2\frac{E_1}{E_3}v_3^1 \\ 0 & 1 \end{Bmatrix} \tag{93}$$

which finally gives :

$$S = \boldsymbol{\beta}\boldsymbol{\alpha}^{-1} = \begin{bmatrix} E_1 & 2\frac{v_3^1}{E_3}E_1 - 1 \\ 1-2v_1^3 & \frac{2}{E_3}\left(1-v_3-2v_3^1 v_1^3\right) \end{bmatrix} \tag{94}$$

In the same way we can provide the expression of the matrix T such that:

$$T \begin{Bmatrix} d\sigma_1' \\ -2d\varepsilon_3 \end{Bmatrix} = \begin{Bmatrix} d\varepsilon_v \\ dq \end{Bmatrix} \tag{95}$$

we build the matrix $\boldsymbol{\alpha}_T$:

$$\begin{Bmatrix} d\sigma_1 \\ -2d\varepsilon_3 \end{Bmatrix} = \boldsymbol{\alpha}_T \begin{Bmatrix} d\sigma_1 \\ d\sigma_3 \end{Bmatrix} = \begin{bmatrix} 1 & 0 \\ 2\frac{v_1^3}{E_1} & 2\frac{1-v_3}{E_3} \end{bmatrix} \begin{Bmatrix} d\sigma_1 \\ d\sigma_3 \end{Bmatrix} \tag{96}$$

and the matrix $\boldsymbol{\beta}_T$:

$$\begin{Bmatrix} d\varepsilon_v \\ dq \end{Bmatrix} = \boldsymbol{\beta}_T \begin{Bmatrix} d\sigma_1 \\ d\sigma_3 \end{Bmatrix} = \begin{bmatrix} \frac{1-2v_1^3}{E_1} & 2\frac{1-v_3-v_3^1}{E_3} \\ 1 & -1 \end{bmatrix} \begin{Bmatrix} d\sigma_1 \\ d\sigma_3 \end{Bmatrix} \tag{97}$$

and we finally get :

$$T = \boldsymbol{\beta}_T\boldsymbol{\alpha}_T^{-1} = \begin{bmatrix} \frac{1-4v_1^3}{E_1} + \frac{2v_1^3 v_3^1}{E_1(1-v_3)} & 2\frac{1-v_3-v_3^1}{1-v_3} \\ 1 + \frac{E_3}{E_1}\frac{v_1^3}{1-v_3} & -\frac{E_3}{2(1-v_3)} \end{bmatrix} \tag{98}$$

with

$$\boldsymbol{\alpha}_T^{-1} = \begin{Bmatrix} 1 & 0 \\ -\frac{E_3}{E_1}\frac{v_1^3}{1-v_3} & \frac{E_3}{2(1-v_3)} \end{Bmatrix} \tag{99}$$
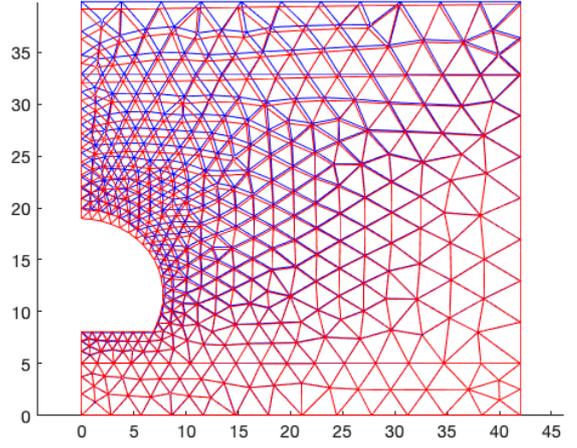
Figure 14. Initial mesh at the beginning of the excavation phase in blue, and deformed mesh (x10) at the end of the excavation phase in red.

	ρ (kg/m^3)	E (MP_a)	v	C (kP_a)	$\phi°$	$\psi°$
top layer	1900	45	0.3	10	30	1
middle layer	2000	200	0.3	20	35	1
bottom layer	2600	1000	0.3	250	20	1

Table 1. Main parameters of the 3 soils and rock layers.

Appendix B.

We present here a finite element simulation of the excavation of a tunnel, using a usual elasto-plastic model based on a Mohr-Coulomb like yield criterion with an isotropic hardening and a non associative flow rule (the Plasol Model (Barnichon [1998])). The principle of the simulation is basic: a first step is done to initialize stresses by gravity loading, then in a second step we remove element of soils that are excavated and decrease progressively reactions forces at the boundary of the created cavity. In the figure 14 the meshes at the beginning and at the end of this second phase are shown. It is constituted of 6 nodes triangles with 7 integration points. The boundary conditions are intuitive: the bottom line is fixed vertically. The left and right vertical lines are fixed horizontally. Three layers of soils are considered. The main mechanical parameters of these three layers are presented in the table 1. In figure 15 we present the maps of the mobilized friction angle divided by the friction angle at failure as well as a map of the local normalized second order work criterion. Finally we present the stress path of one point at the vicinity of the cavity during the excavation phase (see figure 16) to illustrate the fact that the loading direction is not so far from the unloading at constant deviatoric stress analysed in section 3.
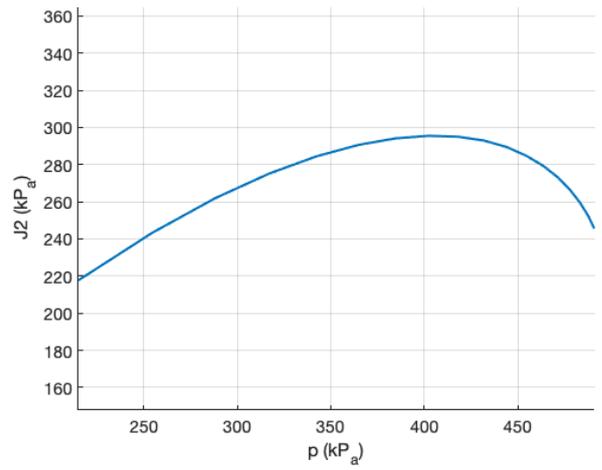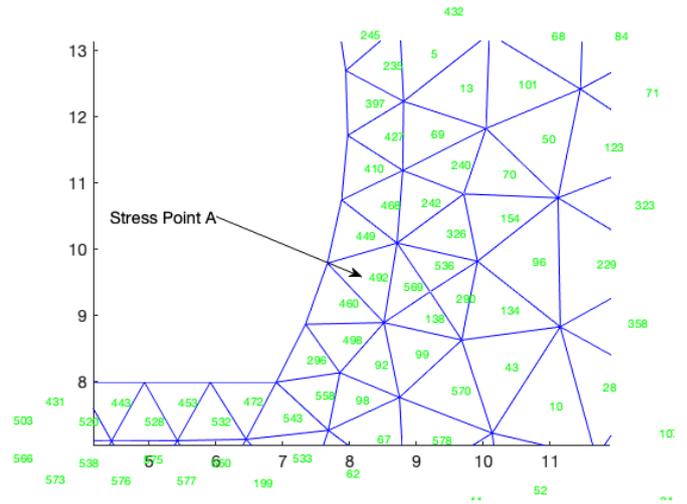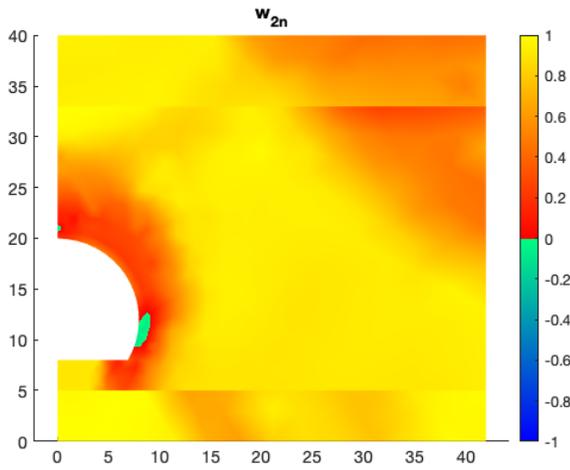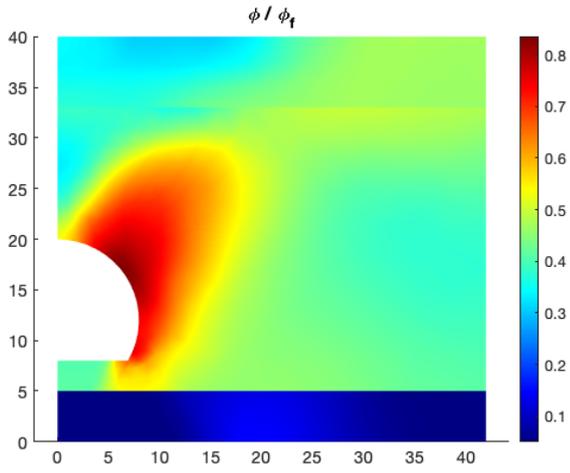
Figure 15. Mobilized friction angle divided by the friction angle at failure (top). Local normalized second order work (bottom).

Figure 16. Loading path of point A during the excavation phase.

Appendix C.

Proof of $w_2 = 0$ inside a localized band.
The Rice (Rice [1976]) localization criterion reads :

$$\det\left(n_i\, M_{ijkl}\, n_l\right) = 0, \qquad \text{with } \vec{n} \neq \vec{0} \tag{100}$$

with $\vec{n}$ the normal vector to the localized band. This last condition is equivalent to :

$$\begin{cases} \exists \vec{g} \neq \vec{0}, \left(\, n_i M_{ijkl} n_l\right)\, g_k = 0 \\ \qquad \Longrightarrow \\ g_j\, \left(n_i\, M_{ijkl}\, n_l\right)\, g_k = 0 \end{cases} \tag{101}$$

In addition, we have :

$$g_j\, \left(n_i\, M_{ijkl}\, n_l\right)\, g_k = 1/2\left(\, n_i\, g_j\, M_{ijkl}\, g_k\, n_l\right) + 1/2\left(\, n_i\, g_j\, M_{jikl}\, \right) \tag{102}$$

due to the minor symmetry of the constitutive matrix. Hence :

$$\begin{cases} g_j\, \left(n_i\, M_{ijkl}\, n_l\right)\, g_k = 1/2\left(n_i\, g_j\, M_{ijkl}\, g_k\, n_l\right) + 1/2\left(g_i\, n_j\, M_{ijk}\right) \\ \qquad = 1/2\left(n_i\, g_j + g_i\, n_j\right) M_{ijkl}\, g_k\, n_l \end{cases} \tag{103}$$

Furthermore, if we state :

$$d\boldsymbol{\varepsilon} = \frac{1}{2}\left(\vec{n} \otimes \vec{g} + \vec{g} \otimes \vec{n}\right) \tag{104}$$

$d\boldsymbol{\varepsilon}$ is a symmetric tensor as well as different from **0** by construction, and :

$$g_j\, \left(n_i\, M_{ijkl}\, n_l\right)\, g_k = d\varepsilon_{ij}\, M_{ijkl}\, g_k\, n_l \tag{105}$$

doing the same for the last two terms on the right, we finally get :

$$\det\left(n_i\, M_{ijkl}\, n_l\right) = 0 \Rightarrow d\varepsilon_{ij}\, M_{ijkl}\, d\varepsilon_{kl} = d\varepsilon_{ij}\, d\sigma_{ij} = 0 \tag{106}$$

inside the localized band.

Appendix D.

In this appendix we present similar results shown in Figure 6 but for the octo-linear model calibrated on the loose Hostun sand.
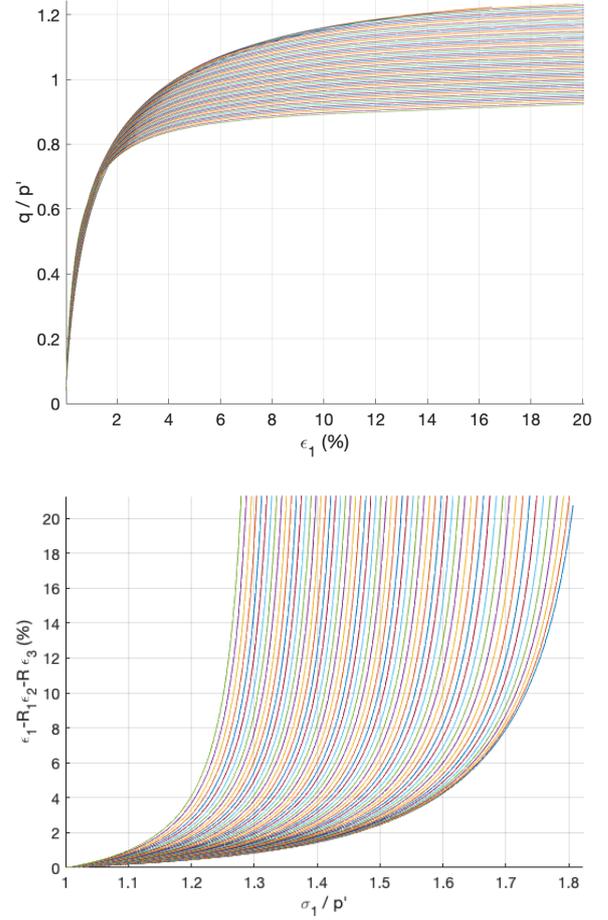
Figure 17. response of the octo-linear model calibrated on a loose Hostun sand to radial loading paths in the deviatoric plane.

Appendix E.

In this appendix we present the results of the simulation presented in section 6, but using the Octolinear model calibrated on a loose sand.
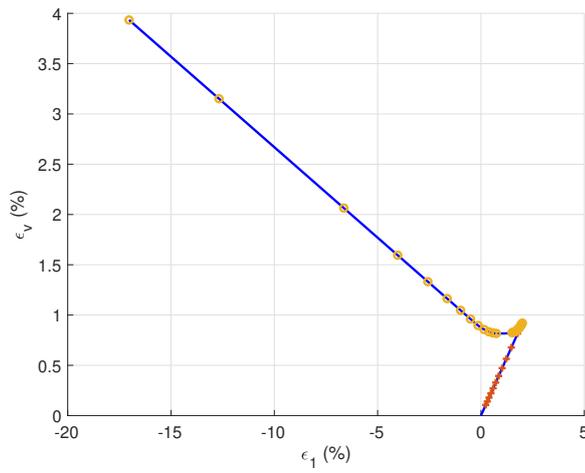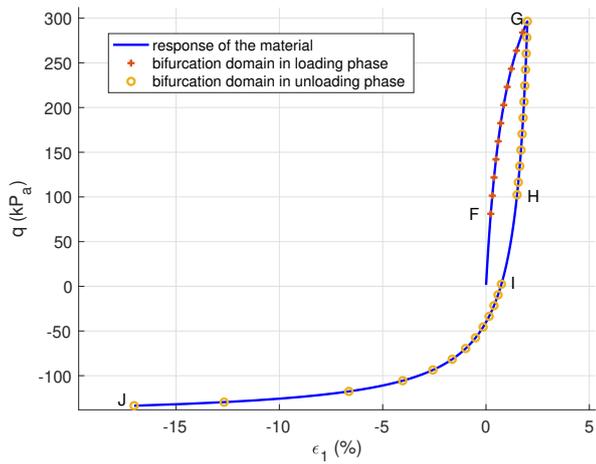
Figure 18. Response of the Octolinear model calibrated on a loose Hostun sand to an alternated drained triaxial path
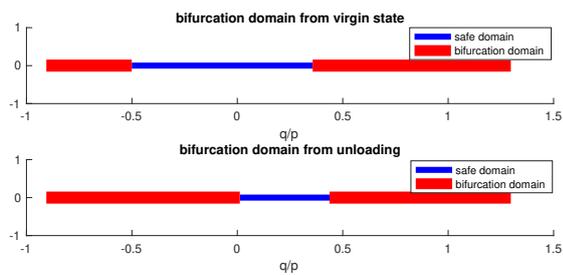
Figure 19. Evolution of the bifurcation domain for a loose sand. At the top, the bifurcation domain obtained starting from the initial isotropic state. At the bottom, the one obtained during the unloading.
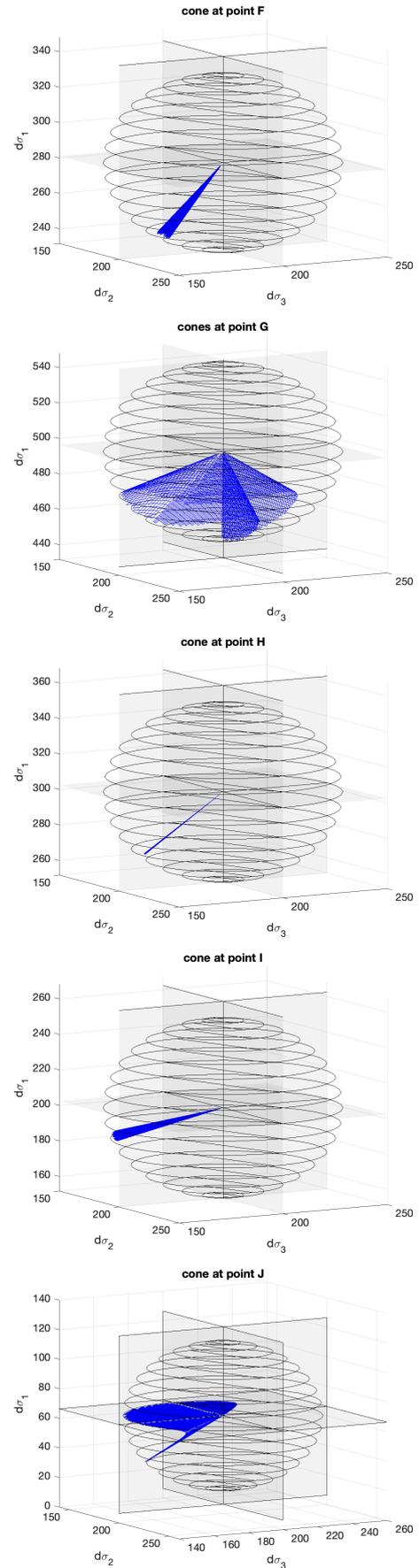
Figure 20. Development of instability cones along the stress path for the loose sand.

Open Geomechanics, 2025, article no. 1

F. Prunier, J. Duriez, L. Sibille & F. Darve, *Characterization of plastic limit surface and bifurcation domain of geomaterials*   17

Appendix F.

Proof of $w_2 = 0$ only at the plasticity limit for generalized $6D$ drained triaxial path in even non orthotropic materials.

Let us consider the general tangent relationship:

$$\begin{Bmatrix} d\sigma_{11} \\ d\sigma_{22} \\ d\sigma_{33} \\ \sqrt{2}d\sigma_{12} \\ \sqrt{2}d\sigma_{23} \\ \sqrt{2}d\sigma_{31} \end{Bmatrix} = \begin{bmatrix} m_{11} & m_{12} & m_{13} & m_{14} & m_{15} & m_{16} \\ m_{21} & m_{22} & m_{23} & m_{24} & m_{25} & m_{26} \\ m_{31} & m_{32} & m_{33} & m_{34} & m_{35} & m_{36} \\ m_{41} & m_{42} & m_{43} & m_{44} & m_{45} & m_{46} \\ m_{51} & m_{52} & m_{53} & m_{54} & m_{55} & m_{56} \\ m_{61} & m_{62} & m_{63} & m_{64} & m_{65} & m_{66} \end{bmatrix} \begin{Bmatrix} d\varepsilon_{11} \\ d\varepsilon_{22} \\ d\varepsilon_{33} \\ \sqrt{2}d\varepsilon_{12} \\ \sqrt{2}d\varepsilon_{23} \\ \sqrt{2}d\varepsilon_{31} \end{Bmatrix} \tag{107}$$

that we rewrite as follows:

$$\begin{Bmatrix} d\sigma_1 \\ d\sigma_i \end{Bmatrix} = \begin{bmatrix} m_{11} & M_{1i} \\ M_{2i} & M_{ii} \end{bmatrix} \begin{Bmatrix} d\varepsilon_1 \\ d\varepsilon_i \end{Bmatrix} \tag{108}$$

with $d\sigma_1 \equiv d\sigma_{11}$, $d\varepsilon_1 \equiv d\varepsilon_{11}$, $d\sigma_i$ and $d\varepsilon_i$ the vectors of 5 components $[22,...,31]$ of $d\boldsymbol{\sigma}$ and $d\boldsymbol{\varepsilon}$ respectively, M_{ii} the 5X5 lower right submatrix, M_{1i} the 1X5 upper right matrix and M_{2i} the 5X1 lower left matrix.

For a generalized $6D$ drained triaxial loading path along direction the direction 1, the vector of components $d\sigma_i$ is a 5X1 zeros vector, thus:

$$w_2 = d\sigma_1 d\varepsilon_1 \tag{109}$$

and by splitting eq.108 into two parts we get

$$d\sigma_1 = m_1 d\varepsilon_1 + M_{1i} d\varepsilon_i \tag{110}$$

$$0_{5x1} = M_{2i} d\varepsilon_1 + M_{ii} d\varepsilon_i \tag{111}$$

From eq.111 we get:

$$d\varepsilon_i = -M_{ii}^{-1} M_{2i} d\varepsilon_1 \tag{112}$$

when M_{ii} is invertible. Including this last expression in eq.110 we come up with:

$$d\sigma_1 = \left(m_{11} - M_{1i} M_{ii}^{-1} M_{2i} \right) d\varepsilon_1 \tag{113}$$

using the Schur's decomposition theorem that stands:

$$\det(m) = \det(M_{ii}) \det\left(m_{11} - M_{1i} M_{ii}^{-1} M_{2i} \right) \tag{114}$$

we finally get:

$$d\sigma_1 = \frac{\det(m)}{\det(M_{ii})} d\varepsilon_1 \tag{115}$$

when M_{ii} is invertible. A a consequence the second order work criterion takes the final form for these particular loading paths:

$$w_2 = \frac{\det(m)}{\det(M_{ii})} (d\varepsilon_1)^2 \tag{116}$$

Hence w_2 vanishes only when $\det(m)$ vanishes, since $d\varepsilon_1 \neq 0$. The permutation over all indices completes the proof.

Conflicts of Interest

The authors declare that there is no conflict of interest. The complete review history is available online.

Acknowledgements

References

Barnichon, J. D. (1998). *Finite element modelling in structural and petroleum geology*. PhD thesis, Université de Liège, Belgique.

Cheng, Z. and Detournay, C. (2021). Formulation, validation and application of a practice-oriented two-surface plasticity sand model. *Computers and Geotechnics*, 132.

Cui, J., Karapiperis, K., Torgersrud, Ø., Andò, E., Viggiani, G., and Andrade, J. (2025). Deciphering necking in granular materials: Micromechanical insights into sand behavior during cycles of triaxial compression and extension. *Journal of the Mechanics and Physics of Solids*, 196.

Dafalias, Y. F. and Manzari, M. T. (2004). Simple Plasticity Sand Model Accounting for Fabric Change Effects. *Journal of Engineering Mechanics*, 130(6):622–634.

Darve, F. and Chau, B. (1987). Constitutive instabilities in incrementally non-linear modelling. In *Constitutive laws for Engineering Materials*, pages 301–310. C. S. Desai.

Darve, F., Flavigny, E., and Meghachou, M. (1995). Yield surfaces and principle of superposition revisited by incrementally non-linear constitutive relations. *International Journal of Plasticity*, 11(8):927–948.

Darve, F., Flavigny, E., and Rojas, E. (1986). A class of incrementally non-linear constitutive relations and applications to clays. *Computers and Geotechnics*, 2(1):43–66.

Darve, F. and Labanieh, S. (1982). Incremental constitutive law for sands and clays: Simulations of monotonic and cyclic tests. *International Journal for Numerical and Analytical Methods in Geomechanics*, 6(2):243–275.

Darve, F., Servant, G., Laouafa, F., and Khoa, H. D. V. (2004). Failure in geomaterials : continuous and discrete analyses. *Computer Methods in Applied Mechanics and Engineering*, 193:3057–3085.

Darve, F. and Vardoulakis, I., editors (2004). *Degradations and instabilities in geomaterials*, volume 461 of *CISM courses*. SPRINGER.

Doanh, T., Dubujet, P., and Protière, X. (2013). On the undrained strain-induced anisotropy of loose sand. *Acta geotecnica*, 8:293–309.

Farahnak, M., Wan, R., Pouragha, M., and Nicot, F. (2024). A multiscale bifurcation analysis using micromechanical-based constitutive tensor for granular material. *International Journal of Solids and Structures*, 298:112866.

Gateaux, R. (1913). Sur les fonctionnelles continues et les fonctionnelles analytiques. *Comptes Rendus Académie des Sciences*, 157:325–327.

Gudehus, G. (1979). A comparison of some constitutive laws for soils under radially loading symmetric loading and unloading. In *Third International conference on numerical Methods in Geomechanics*, pages 1309–1323. Balkema, A. A.

Hill, R. (1958). A general theory of uniqueness and stability in elasto-plastic solids. *Journal of the Mechanics and Physics of Solids*, 6:236–249.

Lade, P. V. (1992). Static instability and liquefaction of loose fine sandy slopes. *Journal of Geotechnical Engineering*, 118(1):51–71.

Lanier, J., Zitouni, Z., Saada, A., Puccini, P., and Bianchini, G. (1989). Comportement tridimensionnel des sables: comparaison d'essais véritablement triaxiaux et d'essais sur cylindre creux. *Rev. Fr. Geotech.*, 49:67–76.

Lyapunov, A. M. (1907). *Annales de la faculté des sciences de Toulouse*, 9:203–274.

Nicot, F. and Darve, F. (2011). Diffuse and localized failure modes, two competing mechanisms. *Internationnal Journal for Numerical and Analitical Methods in Geomechanics*, 35(5):586–601.

Nova, R. (1991). A note on sand liquefaction and soil stability. In 3^{r}d *International Conference on Constitutive Laws for Engineering Materials: Theory and Applications*, pages 153–156.

Nova, R. (1994). Controllability of the incremental response of soil specimens subjected to arbitrary loading programs. *Journal of the Mechanical behavior of Materials*, 5(2):193–201.

Nova, R. (2004). Controllability of geotechnical testing. *Failure, Degradation and Instabilities in Geomaterials. Revue française de génie civil*, 8(5-6):613–634.

Ouadfel, H. and Rothenburg, L. (2001). 'Stress-force-fabric' relationship for assemblies of ellipsoids. *Mechanics of Materials*, 33(4):201–221.

Pastor, M., Zienkiewicz, O. C., and Chan, A. C. (1990). Generalized plasticity and the modelling of soil behaviour. *International Journal for Numerical and Analytical Methods in Geomechanics*, 14:151–190.

Pinzon, G., Ando, E., Desrues, J., and Viggiani, G. (2023). Fabric evolution and strain localisation in inherently anisotropic specimens of anisometric particles (lentils) under triaxial compression. *IGranular Matter*, 298:112866.

Prunier, F., Laouafa, F., and Darve, F. (2009a). 3D bifurcation analysis in geomaterials, Investigation of the second order work criterion. *European Journal of Environmental and Civil Engineering*, 13(2):135–147.

Prunier, F., Laouafa, F., Lignon, S., and Darve, F. (2009b). Bifurcation modeling in geomaterials: from the second-order work criterion to spectral analyses. *International Journal for Numerical and Analytical Methods in Geomechanics*, 33:1169–1202.

Prunier, F., Nicot, F., Darve, F., Laouafa, F., and Lignon, S. (2009c). 3D multi scale bifurcation analysis of granular media. *Journal of Engineering Mechanics (ASCE)*, 135(6):493–509.

Rice, J. R. (1976). The localization of plastic deformation. In Koiter, W. T., editor, 14^{t}h *IUTAM Congress on Theoretical and Applied Mechanics*, pages 207–220.

Sibille, L., Nicot, F., Donzé, F. V., and Darve, F. (2007). Material instability in granular assemblies from fundamentally different models. *International Journal for Numerical and Analytical Methods Geomechanics*, 31(3):457–482.

Wan, R., Nicot, F., and Darve, F. (2017). *Failure in geomaterials, a contemporary treatise*. ISTE-Wiley.

Wang, T., Wautier, A., Tang, C.-S., and Nicot, F. (2024). 3D DEM simulations of cyclic loading-induced densification and critical state convergence in granular soils. *Computers and Geotechnics*, 173.

Zhao, C., Kruyt, N. P., Pouragha, M., and Wan, R. (2022). Fabric response to stress probing in granular materials: Two-dimensional, anisotropic systems. *Computers and Geotechnics*, 146.

Zhu, H., Nguyen, H. N. G., Nicot, F., and Darve, F. (2016). On a common critical state in localized and diffuse failure modes. *Journal of the Mechanics and Physics of Solids*, 95:112–131.

Zorzi, G., Kirsh, F., Gabireli, F., and Rackwitz, F. (2017). Long-term cyclic triaxial tests with DEM simulations. In Wriggers, P, Bishoff, M., Onate, E., Owen, D. R. J., and Zohdi, T., editors, V^th *International Conference on Particle-based Methods - Fundamentals and Applications, PARTICLES 2017*.